Sedimentary Geology
Manuscript Draft

Manuscript Number: SEDGEO6016

Title: The sedimentary controls and reservoir quality implications of modern sand grain coats

Article Type: Research Paper

Keywords: sand grain coat; grain coat formation; reservoir quality; sedimentary controls; modern analogue

Abstract: Clay coated quartz grains can inhibit porosity-reducing quartz cement, and thus can result in unusually high porosity in deeply buried sandstones. Being able to predict the distribution of clay coated sand grains within petroleum reservoirs is thus important to help find unusually good reservoir quality. Here we report a modern analogue study of 12 sediment cores from the Anllóns Estuary, Galicia, NW Spain, collected from a range of sub-environments, to help develop an understanding of the occurrence and distribution of clay coated grain. The cores were logged for grain size, bioturbation and sedimentary structure, and then sub-sampled for electron and light microscopy, laser granulometry, and X-ray diffraction analysis. The Anllóns Estuary is sand-dominated with intertidal sand flats and saltmarsh environments at the margins; there is a shallowing/fining-upwards trend in the estuary-fill succession. Grain coats are present in nearly every sample analysed; they are between 1 µm and 100 µm thick and typically lack internal organisation. The extent of grain coat coverage can exceed 25 % in some samples with coverage highest in the top 20 cm of cores. Samples from muddy intertidal flat and the muddy saltmarsh environments, close to the margins of the estuary, have the highest coat coverage (mean coat coverage of 20.2 % and 21.3 %, respectively). The lowest mean coat coverage occurs in the sandy saltmarsh (10.4 %), beyond the upper tidal limit and sandy intertidal flat environments (8.4 %), close to the main estuary channel. Mean coat coverage correlates with the concentration of clay fraction. The primary control on the distribution of fine-grained sediment, and therefore grain coat distribution, are primary sediment transport and deposition processes that concentrate the clay fraction in the sediment towards the margins of the estuary. Bioturbation and clay illuviation/mechanical infiltration are secondary processes that may redistribute fine-grained sediment and produce grain coats. Here we have shown that detrital grain coats are more likely in marginal environments of ancient estuary-fills, which are typically found in the fining-upward part of progradational successions.

The sedimentary controls and reservoir quality implications of modern sand grain coats

Patrick J. Dowey [a*1], Richard H. Worden[a], James Utley[a], David M. Hodgson[b]

[a]*School of Environmental Sciences, University of Liverpool, 4 Brownlow Street, Liverpool L69 3GP, UK*

[b]*Stratigraphy Group, School of Earth and Environment, University of Leeds, Leeds, LS2 9JT, UK*

[1]*Present address: School of Earth and Environmental Sciences, University of Manchester, M13 9WJ Manchester, UK*

**corresponding author: patrick.dowey@manchester.ac.uk*

Abstract

Clay coated quartz grains can inhibit porosity-reducing quartz cement, and thus can result in unusually high porosity in deeply buried sandstones. Being able to predict the distribution of clay coated sand grains within petroleum reservoirs is thus important to help find unusually good reservoir quality. Here we report a modern analogue study of 12 sediment cores from the Anllóns Estuary, Galicia, NW Spain, collected from a range of sub-environments, to help develop an understanding of the occurrence and distribution of clay coated grain. The cores were logged for grain size, bioturbation and sedimentary structure, and then sub-sampled for electron and light microscopy, laser granulometry, and X-ray diffraction analysis. The

Anllóns Estuary is sand-dominated with intertidal sand flats and saltmarsh environments at the margins; there is a shallowing/fining-upwards trend in the estuary-fill succession. Grain coats are present in nearly every sample analysed; they are between 1 µm and 100 µm thick and typically lack internal organisation. The extent of grain coat coverage can exceed 25 % in some samples with coverage highest in the top 20 cm of cores. Samples from muddy intertidal flat and the muddy saltmarsh environments, close to the margins of the estuary, have the highest coat coverage (mean coat coverage of 20.2 % and 21.3 %, respectively). The lowest mean coat coverage occurs in the sandy saltmarsh (10.4 %), beyond the upper tidal limit and sandy intertidal flat environments (8.4 %), close to the main estuary channel. Mean coat coverage correlates with the concentration of clay fraction. The primary control on the distribution of fine-grained sediment, and therefore grain coat distribution, are primary sediment transport and deposition processes that concentrate the clay fraction in the sediment towards the margins of the estuary. Bioturbation and clay illuviation/mechanical infiltration are secondary processes that may redistribute fine-grained sediment and produce grain coats. Here we have shown that detrital grain coats are more likely in marginal environments of ancient estuary-fills, which are typically found in the fining-upward part of progradational successions.

Keywords: modern analogue; sand grain coat; reservoir quality; sediment controls; grain coat formation

1. Introduction

Clay mineral coats on sand grains can have a significant impact on the pore characteristics of petroleum sandstones reservoirs (Dixon et al., 1989; Bloch et al., 2002; Storvoll et al., 2002;

Geçer Büyükutku and Suat Bağcı, 2005; Berger et al., 2009). Porosity can be reduced and fluid flow restricted where grain coats such as authigenic illite and kaolinite encroach into pore space (Glennie et al., 1978; Seemann, 1979; Kantorowicz, 1990; King, 1992; Waldmann and Gaupp, 2016). Conversely, pore-lining grain coats of chlorite or illite can restrict the growth of pore-filling quartz cement in deeply buried sandstones, thus preserving reservoir quality to greater depths compared with 'clean' sandstones (Bloch et al., 2002; Storvoll et al., 2002). Some of these clay mineral coats originated as detrital coats on sand grains, typically as precursor phases prior to burial, during which they become authigenically altered during burial (Pittman et al., 1992; Wilson, 1994; Bloch et al., 2002; Dowey et al., 2012). Other clay mineral grain coats can develop during burial diagenesis (Burns and Ethridge, 1979; Thomson, 1979; De Ros et al., 1994; Remy, 1994; Anjos et al., 2000; Blackbourn and Thomson, 2000). The term clay coat thus encompasses both detrital and diagenetic origins. Detrital-clay coated grains occur at or near the surface of the sediment, and are the primary focus of this study.

Attempts to predict subsurface authigenic mineral development typically rely on analogue data derived from core (Hassouta et al., 1999; Blackbourn and Thomson, 2000; Schmid et al., 2004) or outcrop (Umar et al., 2011;Henares et al., 2014). Refinement of stratigraphic, sedimentological and mineralogical models occurs through detailed knowledge of time-temperature histories of sedimentary basins (Schneider and Wolf, 2000; Rodrigues Duran et al., 2013) enabling a better understanding of the effects of diagenesis on sandstone (Ramm and Bjørlykke, 1994). An improved understanding of sediment composition in modern environments should give insight into subsequent diagenetic development and thus subsurface reservoir quality (Daneshvar and Worden, in press; Wooldridge et al., in press). It is expected that examining the expression of mineralogy and texture of sediments in modern environments will lead to better understanding of porosity and permeability distribution in ancient and deeply buried reservoirs. The use of modern analogues is common within sedimentology (Eble and Grady, 1993; Edgar et al., 2003; Le Guern and Davaud, 2005 Antrett et al., 2012). However, studies of modern analogues in relation to sandstone reservoir quality are not common (Daneshvar and Worden, in press; Wooldridge et al., in press). This study seeks to address the following research questions:

i) What is the character and degree of coverage of detrital clay grain coats in a modern estuary?

ii) How does grain coat coverage vary between estuarine environments?

iii) What processes control sand grain coat coverage?

iv) How do observed detrital grain coats in modern estuaries relate to grain coats in ancient and deeply buried estuarine sandstones?

2. Grain coat terminology

A range of terms have been used in the literature to describe coats on sand grains that developed pre-, syn- or post-deposition including: “grain coats”, “clay rims”, “inherited clay rims”, “argillans”, “clay skins” “cutans” and “clay coats” ~~(including authigenically~~; Brewer, 1965; Wilson and Pittman, 1977; Pittman et al., 1992; Wilson, 1992; Bloch et al., 2002; Dregne, 2011). Bloch et al. (2002) summarised Wilson and Pittman's (1977) definition of grain coats as “…the result of authigenic processes and form subsequent to burial by growth outward from framework grain surfaces, except at points of grain-to-grain contact.” A further distinction is that “inherited clay rims” are clays present on the grain prior to arrival at the site of deposition (Wilson, 1992). However, Bloch et al.'s (2002) study used the generic term “clay rim” as the authors suggested that coats can also form at the site of deposition following transport (i.e. through infiltration). Here we will use the term "detrital coat", as opposed to "rim" (or clay-rim), since "rim" hints at a two-dimensional coverage (e.g. as observed in thin section), whereas "coat" implies three-dimensional coverage. Furthermore, here we will show that the modern grain coats contain some minerals that are not phyllosilicates (Daneshvar and Worden, in press), and, because "clay" can refer to grain size as well as mineralogy, we have used the term "detrital coat" in preference to "detrital-clay coat".

Modern sandy environments can display variability in the composition and grain size of material within the sediment. Sand-prone, marine-influenced, environments typically contain up to a few percent of silt and clay size detrital minerals and bioclastic material. For this reason, the general term "grain coat" is used here to describe coats on sand grains in both modern and ancient settings. Grain coats can partially or wholly cover the surface of sand grains. The material in the coat may consist of combinations of detrital clay or silt grains, organic matter or mineral precipitates. The coat may develop at any point before deposition, during or immediately after deposition (while still in the original environment of deposition), or after deposition (shallow burial through to late stages of diagenesis). Inherited grain coats can be defined as coats on sand grains that develop prior to deposition during alluvial or fluvial pedogenesis, transport, or transient deposition and early diagenesis en route to the final site of deposition.

We have here proposed firm definitions of terms to be applied to grain coats in sands and sandstones (Table 1); adoption of a common set of terms will help to advance the science by avoiding ambiguity and the proliferation of competing jargon.

3. Study area

The study area is the Anllóns Estuary, Galicia, NW Spain (Fig. 1). This site was chosen for a number of reasons: it has a quartzo-feldspathic rich source mineralogy that is common to a high proportion of sandstone reservoirs, it contains a range of sedimentary environments, and it can be accessed throughout most of the tidal cycle (Barrie et al., 2015). The Anllóns Estuary (Fig. 1) is a relatively deeply incised, partially-filled valley with one large river draining from the east. The Anllóns river drains a 60 km long, 516 km^2 catchment (Varela et al., 2005), and the estuary is microtidal to mesotidal (~1.5 m neap tidal range, ~3.8 m spring tidal range). The area has an oceanic climate, with a mean annual rainfall of 1,000 to 2,000 mm/yr (Arribas et al., 2010). Anthropogenic effects on estuary geomorphology are limited to two managed flood defences in the uppermost estuary reaches (Fig. 1B).

The hinterland geology is dominated by a Devonian to Carboniferous Variscan Orogen, with schistose metasediments, granites, gabbros and basalts (Dallmeyer et al., 1997; Llana-Fúnez and Marcos, 2001). Recent sea level changes have formed a series of drowned, incised valleys, giving this part of the Spanish coast its characteristic wide bays and rias (Alonso and Pages, 2007). A Holocene core in the San Simón Bay (Pérez-Arlucea et al., 2007), approximately 100 km south of the study area, reported two cycles of aggradational channel development followed by abandonment and tidal flat formation. This was succeeded by a phase of incision controlled by sediment supply changes resulting from North Atlantic climate oscillations.

4. Materials & methods

Samples were collected as one-metre long sediment cores. Locations were chosen to cover the range of environments and to result in two transects permitting the construction of correlation panels (Fig. 1B). Twelve cores were collected with a jackhammer-driven window sampler (Van Walt Ltd., 2012). The window sampler works by driving a 50 mm diameter core tube into the sediment. Within the cutting head is a ‘core-catcher’, which keeps the collected core in place and prevents sediment disturbance when the core tube is extracted from the sediment. Sediment cores were collected whole, within a clear polythene liner, enabling the core to be sealed within rigid plastic tubing and transported back to the laboratory. In the laboratory, the core was split into two, logged and the interior of the cores were subsampled for sediment analysis. Care was taken to avoid sample disturbance during sample collection and preparation. A total of fifty-nine subsamples were collected from the cores and used in the study.

Sediment grain-size and sorting were analysed using laser granulometry in a Beckman Coulter LS200 (Beckman Coulter Incorporated, 2011). Sample preparation involved first adding a deflocculant and water to a few grams of the subsample to create a suspension (carbonate was not removed from the sample). The suspension was then added to the laser granulometer where grains were measured based on the diffraction patterns generated when a laser beam was passed through the suspended sediment. Fifty-nine grain size analyses were performed and particles in the size range of 0.4 to 2000 μm were measured.

Measured grain size classes were analysed using Gradistat (version 6) software (Blott, 2008). All grain size and sorting values presented use the modified geometric (Folk and Ward, 1957) graphical measures. An additional measure of the proportion of fine-grained sediment was provided by measuring the relative weight percentage of fine-grained (< 2 µm) sediment within each subsample. Subsamples were weighed and then suspended in water; this suspension was then centrifuged to settle out the > 2 µm (coarse) fraction (Jackson, 1969; Moore and Reynolds, 1997). The suspended finer fraction (< 2 µm) was dried and weighed to enable a weight percentage to be calculated. We have used the Folk and Ward (1957) classifications for grain size, sorting and skewness.

Textural analyses of grain coats on sand grains were performed in a number of ways. Firstly, during sedimentary logging and sampling, whole sediment samples were imaged at low resolution using a standard binocular microscope fitted with a digital camera to qualitatively describe the texture and composition of the sediment. Using this information as a guide, quantitative textural analysis and description was undertaken on whole sediment subsamples using a Philips XL30 scanning electron microscope (SEM) using both secondary electron (SE) and backscatter electron (BSE) modes. Gently disaggregated loose sediment was bonded to an aluminium stub with a carbon sticker, and then covered with a thin veneer of a gold-palladium (80:20 ratio) using a vacuum sputter coater prior to SEM analysis.

Coat coverage on sand grains within each subsample was quantified using SEM analysis. From the subsample of each of the 59 samples, a polished grain-mount section was prepared. Sample preparation involved drying a portion of the subsample at room temperature. Grains were mounted within a plug of epoxy resin under vacuum to prevent spalling of the coat from the grain surface. Resin blocks were then made into standard polished thin sections. Before SEM analysis, the thin section was covered with a thin veneer of carbon using a vacuum carbon coater.

For each sample, sequential high-resolution BSE images of the polished grain mounts were stitched together to form a mosaic of high-resolution images. Individual grain coat coverage was calculated by measuring the proportion of the outer perimeter of the grain that is coated relative to the proportion that is a clean surface. Grain coat coverage is expressed as a percentage, and is therefore independent of grain size. For each sample, one hundred grains were counted, forming a total of 5,900 coat coverage measurements in this dataset. The mean percentage of grain coat coverage was calculated for each sample. An estimate of the precision of the technique was given through the repeated measurement of one image mosaic during the entire sample run; this suggests that the technique produces an error of approximately ± 2 % for the mean grain coat coverage measure.

Random powders from fine fraction samples (< 2 μm) were scanned using a PANalytical X'Pert PRO X-ray diffractometer employing Ni filtered Cu k-α radiation, with a scanning range of 3.9-70.0 °2θ and using extended count times. PANalytical HighScore Plus software permits a semi-quantitative analysis of the minerals present, and produces whole number reports, therefore reporting accuracy is ±0.5%. Samples were then glycolated for twenty-four hours and re-scanned over a range of 3.9 to 13.0 °2θ, to assess the presence of expandable clay minerals (Moore and Reynolds, 1997).

5. Results

5.1. Field description of sedimentary environments

The estuarine sediments analysed in this study are downstream of the managed flood defences where the estuary channel curves 90 degrees towards the southwest (Fig. 1B). In this area, the estuary channel has a variable width (100 to 300 m) with a series of in-channel bars (Figs. 1B & 2A). A large, frontal, attached sandy spit protects the inner portion of the estuary and forces the main estuary channel southward around its tip; the spit is mantled by aeolian dunes (Fig. 1B).

The estuary is sand-dominated throughout. However, field observations of the large-scale geomorphology and smaller-scale sedimentary structures suggested two dominant sub-environments; intertidal flats and saltmarshes (Fig. 1B).

The main occurrence of the saltmarsh is in the middle and upper reaches of the estuary, with a large expanse on the northwestern side of the estuary (Figs. 1B, 2A & B). The saltmarsh has a terraced edge of variable (1 to 2 m) height above the sandflat (Fig. 2B). The saltmarsh is cut by small creeks and channels which fill with water during high tide (Figs. 2A & B). The defining feature of the saltmarsh is that grass covers the majority of the surface and there is visible organic matter within saltmarsh cores. The saltmarsh is visibly low in fine-grained sediment close to the aeolian dune system, and becomes increasingly rich in fine-grained sediment up the estuary. Bioturbation was not observed in saltmarsh sediment.

The intertidal flat occurs close to the main estuary channel with a large expanse in the lower reaches of the estuary. Small meandering tidal streams drain the saltmarsh and incise the intertidal flat (Fig. 2C). The intertidal flats continue around the headland created by the spit and connect with the shoreface at the estuary mouth (Fig. 1B). The intertidal flat is defined by the low coverage of grass and a relative absence of organic matter observable within core samples. The intertidal flat is composed of clean sand close to the main estuary channel and becomes increasingly rich in finer-grained sediment towards the saltmarsh (Fig. 2D & E). The intertidal flats exhibit bioturbation by annelid worms (Fig. 2D & F).

5.2. Laboratory description of sedimentary environments

Laboratory core descriptions have been augmented by determination of fine fraction weight percentages, quantitative coat coverage measurements, and textural and mineralogical analyses. These allowed the saltmarsh and intertidal flat environments to be each sub-divided into two distinct subenvironments, based on the proportion of fine sediment associated with the sand (labelled muddy or sandy). These data are combined below with field observations to describe each of the four sedimentary subenvironments. We have used the Folk and Ward (1957) classifications for grainsize, sorting and skewness. It is noteworthy that all samples from all subenvironments were totally dominated by sand-grade sediment, including the muddy saltmarsh and muddy intertidal flat samples. We will show that most samples have less than 5 % fine fraction, none of the samples contained any mud-dominated matrix material.

5.2.1. Sandy Saltmarsh (SS)

The sandy saltmarsh is characterised by grass covering the majority of the environment surface, and by a high organic matter and low fine-grained sediment concentrations (defined from core samples). The sandy saltmarsh environment is not widespread and is primarily located on the western limit of the estuary close to the aeolian dune system. The sandy saltmarsh is composed of moderately to poorly sorted (mean: poorly sorted) medium sand to silt with symmetrical to very fine skewness (mean: fine). Weight percent fine (< 2 µm) fraction is between 0.4 and 2.2 wt % (mean: 1.2 wt %). Muddy matrix was absent from all sandy saltmarsh samples. Mean sample grain coat coverage ranges from 7.5 to 15.6 % with a mean of 10.4 % (Table 2). Plant roots, woody matter, shell material and sediment mottling are common in core.

5.2.2. Muddy Saltmarsh (MS)

The muddy saltmarsh is also characterised by grass covering the majority of the surface, and by both a high organic matter and high fine-grained sediment concentrations (defined from core samples) (Fig. 2A & B). The muddy saltmarsh is more common than the sand saltmarsh. It forms a narrow strip on the channel bend close to the managed flood defence and follows the course of estuary channel as far as the southerly limit of the saltmarsh. Small areas of the saltmarsh's top surface, close to the intertidal flat, are typically only partly inundated at high tide (particularly during spring tides); these occur as a distinct terrace edge marking the upper limit of the tide on the intertidal flat. Tidal creeks fill with water during the rising tide. Sediment from the muddy saltmarsh consists of moderately to poorly sorted (mean: poorly sorted) medium sands with fine to very fine skewness (mean: very fine). Weight percentage fine fraction (Table 2) is between 1.2 and 22.5 wt % (mean: 5.6 wt %). Loose mud matrix was absent from all samples muddy saltmarsh samples. There were no discrete layers or beds of clay-dominated sediment. Mean sample grain coat coverage ranges from 12.8 to 28.3 % (environment-wide mean: 21.3 %). Plant roots, woody matter and shell material are common.

5.2.3. Muddy Intertidal Flat (MIF)

The muddy intertidal flat is characterised by grass partially covering the surface, and medium organic matter and relatively high fine-grained sediment concentrations (defined from core samples) (Figs. 2C, D & E). The muddy intertidal flat occurs as a 200 to 300 m wide strip oriented parallel with the main channel and saltmarsh environment. This area is covered completely at high tide and is fully exposed at low tide. It is composed of moderate to poorly sorted (mean: poorly sorted) medium sands with fine to very fine skewness (mean: very fine). Weight percentage fine fraction is between 1.9 and 3.9 wt % (mean: 2.6 wt %). Loose mud matrix was absent from all ~~samples~~ muddy intertidal flat samples.There were no discrete layers or beds of clay-dominated sediment. Mean sample grain coat coverage (Table 2) ranges from 9.1 to 30.2 % (environment-wide mean: 20.2 %). Plant roots and shell material are present. Localised sediment mottling is observed in core.

5.2.4. Sandy Intertidal Flat (SIF)

The sandy intertidal flat is characterised by the absence of grass, and by low organic matter and low fine-grained sediment concentrations (defined from core samples) (Fig. 2F & G). The sandy intertidal flat occurs in a strip oriented parallel to the main estuary channel. It is not present on the west side of the upper reaches of the estuary. It develops south of the channel bend (Fig. 1B). Farther downstream, the width of this environment expands south and west of core 24 (50-300 m) where the muddy intertidal flat environment narrows. The sandy intertidal flat is composed of very well to poorly sorted (mean: moderately sorted), fine to medium sands (mean: medium) with coarse to fine skewness (mean: symmetrical). Weight percentage fine fraction (Table 2) is between 0.2 and 1.8 wt % (mean: 0.8 wt %). Muddy matrix was absent from all sandy intertidal flat samples. Mean sample grain coat coverage ranges from 2.3 to 15.6 % (environment-wide mean: 8.4 %). Shell material is common in this environment and localised worm burrows are observed in core.

5.3. Estuary cross-sections

Transects across and down the length of the estuary were constructed to describe the near surface depositional architecture within the estuary. Each transect was hung based on field measurements of surface topography.

5.3.1. Transect one

Transect one (Fig. 3) is relatively short and is aligned northwest to southeast (Fig. 1B). It covers both saltmarsh and intertidal flat environments. The 1 m cores are primarily composed of medium grained sand, although finer grained sediment (silt to clay size), shell material, roots, and plant matter are all present at low concentrations. Core 26 is closest to the main estuary channel and is composed entirely of the sandy intertidal flat (SIF) sediment. Core 27 is more proximal and the lower 80 cm is composed of SIF, this is overlain by a 20 cm wedge of muddy intertidal flat (MIF) sediment. The contact between the MIF and SIF is mapped on the surface of the intertidal flat (Fig. 1). Between cores 27 and 21 there is a small (~ 10 cm) terrace (inset a, Fig. 3). The top of the terrace and core 21 consist of approximately 5 cm of muddy saltmarsh (MS), but beneath this the SIF is exposed. To the northwest, core 29 is composed of sandy intertidal flat in the lower 55 cm. Above this lies 25 cm of MS sediment, which is overlain by 5 cm of sandy saltmarsh (SS).

5.3.2. Transect two

Transect two (Fig. 3) is a long, down-estuary transect from the fluvial end of the estuary (northeast) to a more marine-dominated position (southwest) (Fig. 1B). The cores are primarily composed of medium sand, although finer grained sediment (silt to clay size), shell material, roots and plant matter are all present at low concentrations. The exception to this is core 23, which is composed entirely of SS sediment with interlayers of MS sediment. From core 23, the transect crosses into the estuary channel and down the estuary; at the sediment surface SIF sediment is overlain by MIF sediment. In the lower part of core 30, SIF sediment is split by a shell lag layer overlain by 40 cm of muddy intertidal flat sediment. The shell lag layer is composed primarily of disarticulated shells and shell fragments, the only occurrence of this encountered in the cores. The shell lag is therefore interpreted to be localised, as opposed to estuary-wide. Downstream, core 27 marks the intersection of transects 1 and 2. Between cores 30 and 27 the MIF sediment thins to approximately 20 cm. Core 24 is furthest down the estuary and closest to the open ocean, and the muddy intertidal flat environment is not expressed on the surface of the sediment. However, there is a thin lens of MIF about 10 cm below the surface that may link with the thicker section of muddy intertidal flat sediment at depth in core 27.

5.4. Grain coat textural and compositional characteristics

Low resolution binocular microscope examination revealed that a minority of sand grains have up to one quarter of the surfaces coated in fine grained material. Samples with the greatest amounts of grain coating materials come from sediment with highest fines content. Grain coats appear as dark brown, fine-grained (clay to silt size) material on the grain surfaces (Figs. 4A & B). Sand grains that hosted coats were primarily round to sub-round, and the majority of grains were quartz, with subordinate amounts of feldspar. Carbonate bioclasts were also present. Detrital mineral grains such as mica and chlorite could not be identified using the binocular microscope.

Sediment was taken from the interior of freshly opened damp cores with no sample disturbance. The heat of the microscope lamp quickly dried the sediment, resulting in a hard and brittle mass consisting of both grains and grain coats. No matrix was observed in any damp or dry sediment samples from any of the cores, including the muddy saltmarsh sediments (Figs 4A to D). This observation demonstrates that grain coats, quantified later using polished sections and SEM examination, are not primary matrix that has subsequently adhered to grains during sample preparation.

With a binocular microscope at high magnification (Figs. 4C & D), it was possible to view individual grains and plant matter within the coating material. At this scale of resolution a qualitative assessment of grain coat completeness (0 to 100 %) and thickness (1 to 100 µm) was recorded.

Using polished section grain mounts in the SEM in backscattered imaging mode; it was found that some degree of grain coat is present on most grains (Figs. 5, 6 & 7). Mean coat coverage in some samples exceeds 25 % of the grain perimeter, but is typically in the range 0-15 % (Fig. 8). Grain coat coverage tends to increase up through the core samples (Fig. 8). The average grain coat coverage of all grains measured in the dataset is 11.4 %. The thickness of coats ranges from 1 µm up to 100 µm. Coats observed in polished section display no internal structure or systematic organisation (Fig. 5E-H). Grain coats are composed of fine minerals, consisting primarily of clay minerals plus silt-size detrital grains, carbonate fragments and pyrite grains (Fig. 6B, F & J). High-resolution stub-mounted samples revealed that the fine-grained material in the grain coats is predominantly composed of clay minerals (Fig. 6C, G & K).

Compositional analysis of coats was undertaken using secondary X-ray spectra (EDX) on both stub and thin section grain mounts (Figs. 6 & 7). However, EDX analysis of stub-mounted coats proved difficult due the fine grained nature of the grain coats. EDX analysis of grain coats in polished section grain mounts was successfully undertaken and provided unequivocal (i.e. single-mineral) analyses of: chlorite $(Fe,Mg_5Al)(AlSi_3)O_{10}(OH)$ (Figs. 7A-C), illite ($KAl_3Si_3O_{10}(OH)_2$), (Figs. 7D-F) gibbsite ($Al(OH_3)$) (Figs. 7G-I) and kaolinite ($Al_2Si_2O_5(OH)_4$) (Figs. 7J-O).

Mineral composition of the coats from the fine sediment fraction (<2 µm) of the samples was determined using XRD (Fig. 9 & supplementary online data). The fine sediment fraction (Fig. 9A-B) predominantly consists of a mixture of sheet silicates, framework silicates (quartz and feldspar) and carbonates (dolomite and calcite). Although there is significant spread between environments, the fine fraction of samples from the sandy intertidal flat and muddy intertidal flat environments are predominantly carbonate- and framework silicate-rich, while those from the muddy saltmarsh and sandy saltmarsh environments are sheet silicate- and framework silicate-rich. The concentrations of sheet silicates are tightly clustered with high proportion of muscovite/illite (35-60 %) and lesser proportions of chlorite (15-25 %) and kaolinite (15-45 %). Eight out of fifty-nine fine fraction separates consist of 100 % muscovite/illite.

6. Discussion

6.1. Core & transects interpretation

Estuary transects allow the development of a stratigraphic framework from which the distribution of grain coats can be mapped and which may help to identify the key processes that control the grain coat distribution. There are two saltmarsh environments: muddy saltmarsh (MS) and sandy saltmarsh (SS). In the upstream section of the estuary (Fig. 3), the saltmarsh cores (e.g. core 23) are SS sediments at the base that fine upwards to MS sediments. In the centre of the estuary, the lower sections of cores 29 and 21 consist of sandy intertidal flat (SIF) overlain by MS sediment. In core 29 this SIF-MS package is overlain by a thin veneer of SS, which may be the result of windblown sand from nearby aeolian dunes. The saltmarsh setting (MS and SS) is interpreted to be a supratidal environment that only floods during spring (large amplitude) tides.

Sandy intertidal flat environments dominate the estuary. The proximity of the SIF environments to the main tidal channel, the low fines content and the lack of internal sedimentary structures indicate that it is subject to tidal and marine reworking. A spatially restricted shell lag, interpreted to be the localised infill of a small channel scour or the remnant of a storm event, occurs within one core (Fig. 3).

The muddy intertidal flat (MIF) is composed of fine-grained and generally poorly sorted sands. Combined~~,~~ with field observations, this indicates that the MIF environment represents a lower energy setting than the SIF environment. The MIF occurs in the upper tidal zone of the estuary where low flow velocities during high tide slackwater permit fine-grained sediment deposition. During falling tides, flow velocities are initially too low to resuspend fine-grained sediment. However, during the falling tide flow velocities will continue to increase ultimately resuspending fine-grained sediment. This will occur at a line close to the intersection of the surficial contact of the MIF and SIF. The MIF environment marks a zone of net fine-grained sediment deposition, in contrast to the SIF where fine-grained sediments are subject to reworking, resuspension and transportation. This process has been noted in the formation of tidal mudflats (Allen, 2000), and is enhanced by plant colonisation (Fig. 2C), which can bind cohesive sediment together and reduce tidal velocities.

An overall fining- and shallowing-upwards stratigraphic trend is indicated by the development of the MIF on top of the SIF, and of both saltmarsh environments developed on top of the intertidal environments (Figs. 1 & 3). This shallowing- and fining-upwards trend is supported by the observation that fine fraction content increases in the shallowest 20 cm of the most cores (Fig. 8). Furthermore, the partial colonisation of the MIF environment by plants (Fig. 2C) could be the first stage of saltmarsh development in this area (French, 1993; Allen, 2000). The timescale of this change is not currently known, but likely occurred during the Holocene (Pérez-Arlucea et al., 2007), or more recently due to anthropogenic influence. There are several potential causes of the fining- and shallowing-upwards trend: 1) sediment progressively infilling the estuary, 2) changes in sediment patterns resulting from anthropogenic influences, or 3) change in sediment grain size or volume caused by climate oscillations.

The changes in sediment observed in the estuary are of a limited vertical extent (< 2 m), and the stratigraphic response of the estuary to Holocene sea level fluctuations is outside the scope of this study. However, fining-upwards patterns are typical of the upper part of many tide-influence systems (Weimer et al., 1982; Kitazawa, 2007). Progradation, and shallowing, at the estuary margins indicates that sediment supply is outpacing relative sea-level rise. Holocene relative sea level rise had an impact on the development of European coastal systems (Allen, 2003; Tessier et al., 2012; Fanget et al., 2014). Progressive infilling of the estuary could have resulted from sediment brought onshore (Harris, 1988; Woodroffe et al., 1993; Boski et al., 2002).

The fining and shallowing trend observed may be due to changes in sediment patterns caused by anthropogenic influences. Upstream of the estuary, the creation of small, localised flood defences (Fig. 1A) may have somewhat influenced sedimentation patterns. During high tide, the flood defences become inundated with estuary waters, which would have previously pushed further upstream. This change will reduce tidal velocities behind the upstream-moving mixing zone, which in turn could result in reduced fine-grained sediment resuspension on the intertidal flat and the development of the MIF environment.

A change in sediment grain size or quantity caused by climate oscillations could also produce the observed fining-upward trend, either due to an increase in fine sediment or a decrease in sand from marine or fluvial sources (Orton and Reading, 1993; Reading and Collinson, 1996). In the nearby San Simón Bay estuary, Holocene climate oscillations changed the overall volume of sediment which, in turn had an effect on the depositional environments (Pérez-Arlucea et al., 2007). Reportedly colder and wetter climates resulted in increased sediment supply, the infilling of estuarine channels and the formation of estuarine tidal flats. The fining- and shallowing-upward trend may also result from changes in sediment grain size or volume caused by modifications in anthropogenic land use such as land clearance or mining (Walling, 1999, 2006).

6.2. Grain coat coverage and mineralogy

Grain coat coverage measurements were averaged for each sample and for each environment of deposition. Sample mean grain coat coverage data for each sample have been compared to grain size, fine fraction quantity, skewness of grain size and sorting (Fig. 10A to D).

Analysis of variance calculations indicate that the differences in mean coat coverage between each of the environment-wide mean values (Table 2) are statistically significant (see supplementary data).

There is no relationship between mean coat coverage and grain size (Fig. 10A). However, there are weak, positive correlations (r = 0.6 to 0.7) between mean coat coverage and fine fraction content, skewness and sorting (Fig. 10B-D). Figures 10B-D also demonstrate~~s~~ that mean sample grain coat coverage in SIF and SS environments are commonly lower than in the MIF and MS environments.

Fine fraction weight percent and mean coat coverage percentage vary with depth (Fig. 8). Ten cores have the highest fine fraction content in the top 20 cm of the core. Fine fraction content generally decreases with depth in all of the cores, except cores 28 and 31. Mean coat coverage in each of the cores follows a similar pattern, with highest coat coverage in the upper 20 cm of the sediment in six of the cores. Mean coat coverage decreases with depth in nine of the ten cores.

The mineralogy of grain coats in intertidal flat environments (Fig. 9A) largely reflects high energy conditions with the high concentrations of carbonate and framework silicates. Conversely, the mineralogy of grain coats in saltmarsh environments reflects low energy conditions with high concentrations of sheet and framework silicates. The tight clustering of the varieties of sheet silicates in grain coat fine fractions across the range of environments (Fig. 9B) is interpreted to reflect a consistency in mineral distributions. This suggests that sheet silicates are either supplied from similar sources (bedrock and hinterland sediments) or are evenly distributed throughout the estuary by sedimentary transport processes. Carbonate is supplied from marine sources. Framework silicates, chlorite and muscovite are present within basinal bedrock sources (Calvo et al., 1983; Dallmeyer et al., 1997; Llana-Fúnez and Marcos, 2001). Kaolinite is likely to result from the weathering of basinal bedrock (Deer et al., 1992; Fernández-Caliani et al., 2010; Wilson, 1998).

6.3. Grain coat formation

Based on previously published mechanisms, there are two possible causes of grain coats ~~have~~ in the Anllóns estuary: bioturbation (Needham et al., 2005; Worden et al., 2006) and mechanical infiltration or illuviation (Buurman et al., 1998). It should be noted that the grain coats are definitely not an artefact resulting from any mud matrix that has adhered to the grains during drying of the samples since there was no mud matrix in any of the samples (Figs. 4 to 7).

Large scale bioturbation of intertidal flat sediment (Figs. 2C to E) by *Arenicola* (the common lugworm) leaves excreted sediment mounds on the sediment surface (Wooldridge et al., in press). Laboratory experiments during which *Arenicola marina* worms bioturbated artificially interbedded sands and a mixture of crushed slate and organic matter (Needham et al., 2005; Worden et al., 2006) demonstrated that coats on sand grains can be created through this process. As the worm ingests, digests and then excretes the sand and fine-grained sediment, they become mixed together. A sticky mucous membrane produced in the guts of the worm results in the fine-grained sediment adhering to the surface of the sand grain. It was also noted that the acidic environment within the worm’s guts resulted in the dissolution of feldspar and the formation of a suite of clay minerals (Needham et al., 2006; Worden et al., 2006).

Coats produced during experimental bioturbation are strikingly similar to those observed in the Anllóns estuary, with comparable morphology and grain coat thickness (a few 10's of µm) and an absence of an internal structure. *Arenicola* worms occur in great abundance at some locations on the muddy intertidal flat (MIF), particularly where clay and silt grade sediment is at its highest concentration. The higher fine fraction concentration and mean coat coverage in the upper few centimetres suggest that the coating mechanism occurred near to the sediment surface (Fig. 8). This distribution is likely because organic matter (which worms use as food) and fine-grained sediment have low densities and may be deposited in similar locations. Furthermore, clay minerals and organic matter are more likely to be co-deposited because they typically form aggregates in the water column (Kranck, 1973; Eisma, 1986; Burban et al., 1990). When sandy sediment, with an overlying veneer of fine-grained sediment and organic matter, is bioturbated, it may result in the formation of grain coats on individual sand grains. Although a mucous membrane was not observed with the analytical techniques available, worm secretion possibly adhered the coating material to the grain.

Wilson (1992) identified similar grain coat features as “*inherited clay rims*”. These were reported to result from both the reworking of partially-cemented grains formed in contemporary aeolian and sabkha deposits and through the ingestion of sediment by organisms in shelf settings. In the latter case, given the variety and range of bioturbating organisms in sedimentary environments (Knaust and Bromley, 2012), it seems unlikely that this process is limited exclusively to shelf environments.

Other than bioturbation, clay illuviation/mechanical infiltration could produce the grain coats observed. Within the geological and soil literature two processes have been defined (Buurman et al., 1998). These processes have been given different names but are essentially the same. Mechanical infiltration is interpreted to have occurred primarily in ancient sandy desert and river settings (Walker et al., 1978; Moraes and De Ros, 1990, 1992; Weibel, 1998; Du Bernard and Carrio-Schaffhauser, 2003; Ketzer et al., 2005); while clay illuviation is widely reported in modern sandy soils (Kuhn et al., 2010).

Mechanical infiltration has been defined in geological literature as the process of sediment-laden water entering a sandbody and depositing fine clay size particles onto framework grain surfaces. Deposition of fine-grained sediment on sand grain surfaces can result from the evaporation of the water, a reduction in flow velocity, or percolating water encountering a barrier (Moraes and De Ros, 1990). Although this process has been interpreted primarily in desert and river settings, it plausibly occurs in most sandy environments that experience ephemeral water flow (including estuaries). An ancient example is the Jurassic fluvial Sergi Formation, Brazil (Moraes and De Ros, 1990, 1992), in which clay minerals between sand grains formed a range of textures including grain-bridges, geopetal fabrics, loose aggregates and coats (cutans). These sandstone clay mineral fabrics were reported to have developed in a semi-arid area with a lowered water table, where episodic runoff was able to infiltrate coarse sands. Clay mineral concentrations were noted to decrease away from possible fluid entry points.

Clay illuviation has been defined in soil literature as the transportation of clay grade sediment (eluviation) from a surface or near-surface soil layer and subsequent accumulation (illuviation) in an underlying layer (Kuhn et al., 2010). Such coats typically occur in 'channels' within the soil pore volumes (Miedema et al., 1999). Although coarse coats can develop (McKeague et al., 1971; Kemp et al., 1998), illuviated coats typically tend to be fine-grained, with repeated growth of coats producing laminations (Miedema et al., 1999; Kuhn et al., 2010). As outlined by Buurman et al. (1998) mechanical infiltration and clay illuviation appear to be similar. However, there are differences in the source of the suspended material in mechanical infiltration (runoff/streamflow) versus clay illuviation (overlying soil layer) and in the textures of the coats.

Twice daily tides cover the majority of the intertidal flat in the Anllóns estuary. The rising tide results in the flow of estuarine waters through previously-drained pores between sand grains on the uppermost part of the intertidal flat. As the tide falls below the sediment surface, water drains out through the pores between the sand grains. Where fine-grained sediment is transported by tidal waters, intertidal sands may act as a filter, trapping fine-grained sediment at the interstices between sand grains or where pore throats are narrow, thus possibly resulting in the formation of grain coats on the surface of sand grains. Suspended sediment may be sourced from both the veneer of fine-grained sediment deposited after high tide, and from turbid estuary waters. For the former source, on a falling tide, water in the upper part of the intertidal flat (MIF) could be drawn down (Santos et al., 2012), resuspending and transporting fine-grained sediment into the underlying sandbody. For the latter source, fine-grained sediment suspended in estuary waters above the sediment surface could be drawn into the tidal sandbody due to processes similar to tidal pumping (Santos et al., 2012).

The higher fine fraction concentration and mean coat coverage in the upper few centimetres (Fig. 8) support the interpretation that coats developed near to the sediment surface (Fig. 8). Tidal pumping may be more likely to occur at the margins of the estuary (muddy intertidal flat) where the surface elevation is typically higher than the sandy intertidal flat (Fig. 3). In the Anllóns estuary, grain coats lack internal textures (Figs. 5 to 7). Kuhn et al. (2010) identified laminar coats developed due to repeated cycles of suspended sediment flow. The tidal cycle within the estuary would seem likely to produce laminated coats. However, the lack of laminated grain coats could be due to the relatively low volumes of suspended fine-grained sediment (<6 wt %) from which the coats form (Fig. 10B).

Either bioturbation, mechanical infiltration/clay illuviation, or a combination of both processes, may produce the observed sand grain coats in the Anllóns estuary.

To identify which process occurs, or is dominant, may require further detailed analysis to identify either the presence of biofilms (Allen and Duffy, 1998) or to identify locations of laminar textures in sand grain coats. However, it is clear from the geographic spread, and their near-ubiquitous presence, that grain coats are an important component of the sediment character in the estuary. The high mean grain coat coverage and fine fraction concentration in the upper 20 cm of the core indicate that the processes that produce grain coats occurs at the surface of the estuary.

6.4. Predicting sand grain coats

Locating the environments where the greatest sand grain coat coverage occurs in modern settings is useful because it may indicate where grain coats are more likely to be present in ancient and deeply buried reservoir facies. In the Anllóns estuary (Fig. 1), on the sandy intertidal flat (SIF) medium sands are moderately-sorted and mean fine fraction content is 0.8 %. On the muddy intertidal flat (MIF) the medium sands are poorly sorted with a mean fine fraction content of 2.6 %. The less than 2 % difference in fine fraction content produces a difference in mean coat coverage of approximately 11 %. This difference in mean coat coverage seems likely to be related to the position of the environment within the estuary. Close to the estuary channel, flow velocities are too great to deposit sufficient fine-grained sediment (that can then be incorporated into grain coats), but at the margins of the estuary flow velocities are lower and fine sediment can be deposited.

From this observation, combined with the Dalrymple et al. (1992) estuary classification scheme, it is possible to develop a model (Fig. 11) for the distribution of grain coats on sand grains. As in the Anllóns estuary, the model is a hybrid wave- and tide-dominated estuary with a barrier separating the central basin. Sandy and muddy intertidal flats within the estuary are dissected by channels and drainage creeks. Mean low tide is marked by the larger subaqueous channels and creeks. Mean high tide is the top surface of the saltmarsh, beyond which is only reached by spring tides. The intertidal flat is split into two areas; the sandy intertidal flat proximal to the mouth of the barrier, and the larger estuary channels. Moving toward the margins of the estuary, the muddy intertidal flat (MIF) is a lower energy area close to the mean high tide limit. This MIF area is more likely to have sufficient fine-grained sediment deposited to provide the source material for grain coats to develop. Flow velocities will be low enough for fine-grained sediment deposition and to prevent resedimentation and reworking in normal estuary conditions.

Fine fraction content and mean grain coat coverage values are at their highest in the upper part of the sediment (Figs. 10 & 11). In this zone the processes that may lead to the fine-grained sediment being ‘glued-on’ to sand grains occur: (i) bioturbation, due to the high organic content and a lower energy setting and (ii) clay illuviation/mechanical infiltration because of the presence of fine-grained sediment and potential tidal pumping processes. Assuming that grain coats are retained in the sediment after their formation, it may be expected that grain coats could occur preferentially in the upper parts of fining-upwards sets or parasequences. Parasequences mark periods of progradation and do not typically form good reservoir units (Bridge and Demicco, 2008). The presence of grain coats on sand grains in these settings may therefore have a negative impact on reservoir quality in sandstones.

7. Conclusions

1. The grain coats in the Anllóns estuary, NW Spain, have a wide geographic and environmental spread within the estuary and are best developed in the upper 20 cm of the cores studied.

2. Grain coats are present in all cores and nearly every sample analysed, and therefore are an important component of the estuary-fill.

3. Grain coat thickness is variable (1 to 100 µm) and grain coats have no internal texture or organisation.

4. Grain coats are partially developed on most grains, with mean coat coverage exceeding 25 % in some samples. The highest mean coat coverage occurs in the muddy intertidal flat environment (24.1 %) and the muddy saltmarsh environments (24.8 %) on the margins of the estuary. The sandy saltmarsh has average coat coverage ranges of 16.0 %. The lowest average grain coat coverage range is within the sandy intertidal flat environment (13.5 %), which tends to occur closest to the main estuary channel and at depth in cores.

5. Mean coat coverage correlates with the fine fraction concentration, skewness and sorting in the sediment. Mean coat coverage does not correlate with grain size. Grain coats are composed of a range of material: sheet silicates (muscovite, chlorite and kaolinite), framework silicates (quartz and feldspar) and carbonate (calcite and aragonite).

6. The primary controls on the distribution of fine-grained sediment, and therefore grain coat distribution, are transport processes, which concentrate fine-grained sediment at the margins of the estuary. Secondary processes that may produce grain coats are likely to be: (i) sediment bioturbation, which may adhere fine-grained material on to sand grains, and/or (ii) mechanical infiltration/clay illuviation of fine-grained sediment.

7. By analogy to the work on a modern example presented here, grain coats are more likely to occur in areas within ancient, deeply buried estuarine sandstone reservoir that are close to the upper tidal limit. This is where fine-grained sediment is concentrated during deposition and where bioturbation or mechanical infiltration/clay illuviation may be more common.

Acknowledgements

Gemma Barrie and Ehsan Daneshvar are thanked for their efforts in collecting sediment samples. The members of the first Chlorite Consortium at Liverpool University (BP, Chevron, ConocoPhillips, Eni, ExxonMobil, Petrobras, Statoil and Shell) are warmly thanked for supporting this work. The initial encouragement of Andy Thomas and Joann Welton was instrumental in getting this research off the ground. Joanna Ajdukiewicz is thanked for discussions on grain coat quantification. Natasha Dowey is thanked for text edits.

Supplementary data

Supplementary data associated with this article can be found in the online version, at: ##insert URL##. These data include grain coat coverage statistical analysis and grain coat XRD mineralogy.

References

Adams, R.S., Bustin, R.M., 2001. The effects of surface area, grain size and mineralogy on organic matter sedimentation and preservation across the modern Squamish Delta, British Columbia; the potential role of sediment surface area in the formation of petroleum source rocks. Int. J. Coal Geol. 46, 93–112.

Allen, J.R.L., 2000. Morphodynamics of Holocene salt marshes: A review sketch from the Atlantic and Southern North Sea coasts of Europe. Quat. Sci. Rev. 19, 1155–1231.

Allen, J.R.L., 2003. An eclectic morphostratigraphic model for the sedimentary response to Holocene sea-level rise in northwest Europe. Sediment. Geol. 161, 31–54. doi:http://dx.doi.org/10.1016/S0037-0738(02)00394-9

Allen, J.R.L., Duffy, M.J., 1998. Temporal and spatial depositional patterns in the Severn Estuary, southwestern Britain: intertidal studies at spring-neap and seasonal scales, 1991-1993. Mar. Geol. 146, 147–171.

Alonso, A., Pages, J.L., 2007. Stratigraphy of Late Pleistocene coastal deposits in Northern Spain. J. Iber. Geol. 33, 207–220.

Anjos, S.M.C., De Ros, L.F., Schiffer de Souza, R., Assis Silva, C.M., Sombra, C.L., 2000. Depositional and diagenetic controls on the reservoir quality of Lower Cretaceous Pendencia sandstones, Potiguar rift basin, Brazil. Am. Assoc. Pet. Geol. Bull. 84, 1719–1742.

Antrett, P., Vackiner, A.A., Kukla, P.A., Back, S., Stollhofen, H., 2012. Controls on reservoir compartmentalization of an Upper Permian tight gas field in Germany and links to a modern analogue in the Western US. Pet. Geosci. 18, 289–304. doi:10.1144/1354-079311-037

Arribas, J., Alonso, Á., Pagés, J.L., González-Acebrón, L., 2010. Holocene transgression recorded by sand composition in the mesotidal Galician coastline (NW Spain). The Holocene 20, 375–393. doi:10.1177/0959683609353429

Barrie, G.M., Worden, R.H., Barrie, C.D., Boyce, A.J., 2015. Extensive evaporation in a modern temperate estuary: Stable isotopic and compositional evidence. Limnol. Oceanogr. 60, 1241–1250.

Beckman Coulter Incorporated, 2011. Coulter LS series: Product manual.

Berger, A., Gier, S., Krois, P., 2009. Porosity-preserving chlorite cements in shallow marine volcaniclastic sandstones: Evidence from Cretaceous sandstones of the Sawan gas field, Pakistan. Am. Assoc. Pet. Geol. Bull. 93, 595–615.

Blackbourn, G.A., Thomson, M.E., 2000. Britannia Field, UK North Sea: petrographic constraints on Lower Cretaceous provenance, facies and the origin of slurry-flow deposits. Pet. Geosci. 6, 329–343.

Bloch, S., Lander, R.H., Bonnell, L., 2002. Anomalously high porosity and permeability in deeply buried sandstone reservoirs: Origin and predictability. Am. Assoc. Pet. Geol. Bull. 86, 301–328.

Blott, S.J., 2008. Gradistat V. 7.

Boski, T., Moura, D., Veiga-Pires, C., Camacho, S., Duarte, D., Scott, D.B., Fernandes, S.G., 2002. Postglacial sea-level rise and sedimentary response in the Guadiana Estuary, Portugal/Spain border. Sediment. Geol. 150, 103–122. doi:http://dx.doi.org/10.1016/S0037-0738(01)00270-6

Brewer, R., 1965. Fabric and mineral analysis of soils. Soil Sci. 100, 73.

Bridge, J., Demicco, R., 2008. Coasts and shallow seas, in: Earth Surface Processes, Landforms and Sediment Deposits: Cambridge University Press, Cambridge, pp. 473–562. doi:10.1017/CBO9780511805516.016

Burban, P.-Y., Xu, Y.-J., McNeil, J., Lick, W., 1990. Settling speeds of flocs in fresh water and seawater. J. Geophys. Res. 95, 18,213-218,220.

Burns, L.K., Ethridge, F.G., 1979. Petrology and diagenetic effects of lithic sandstones: Paleocene and Eocene Umpqua Formation, southwest Oregon, in: Scholle, P.A., Schluger, P.R. (Eds.), Aspects of Diagenesis. SEPM Special Publication 26. Society of Economic Paleontologists and Mineralogists, Tulsa, Oklahoma, pp. 307–317.

Buurman, P., Jongmans, A.G., PiPujol, M.D., 1998. Clay illuviation and mechanical clay infiltration - is there a difference? Quat. Int. 51–52, 66–69.

Calvo, R.M., Garcia-Rodeja, E., Macias, F., 1983. Mineralogical variability in weathering microsystems of a granitic outcrop of Galicia (Spain). Catena 10, 225–236. doi:10.1016/0341-8162(83)90033-4

Dallmeyer, R.D., Martínez Catalán, J.R., Arenas, R., Gil Ibarguchi, J.I., Gutiérrez Alonso, G., Farias, P., Bastida, F., Aller, J., 1997. Diachronous Variscan tectonothermal activity in the NW Iberian Massif: Evidence from 40Ar/39Ar dating of regional fabrics. Tectonophysics 277, 307–337. doi:10.1016/s0040-1951(97)00035-8

Dalrymple, R.W., Zaitlin, B.A., Boyd, R., 1992. Estuarine facies models: conceptual basis and stratigraphic implications. J. Sediment. Petrol. 62, 1130–1146.

Daneshvar, E., Worden, R.H., n.d. New approaches for understanding provenance controls on feldspar alteration in sediments: implications for reservoir quality, in: Armitage, P.J., Butcher, A., Churchill, J., Csoma, A., Hollis, C., Lander, R.H., Omma, J., Worden, R.H. (Eds.), Reservoir Quality Prediction in Sandstones and Carbonates. Geological Society Special Publication.

De Ros, L.F., Anjos, S.M.C.C., Morad, S., 1994. Authigenesis of amphibole and its relationship to the diagenetic evolution of lower cretaceous sandstones of the Potiguar rift basin, northeastern Brazil. Sediment. Geol. 88, 253–266. doi:10.1016/0037-0738(94)90065-5

Deer, W.A., Howie, R.A., Zussman, J., 1992. An Introduction to the Rock-Forming Minerals, 2nd ed. Longman.

Dixon, S.A., Summers, D.M., Surdam, R.C., 1989. Diagenesis and preservation of porosity in Norphlet Formation (Upper Jurassic), Southern Alabama. Am. Assoc. Pet. Geol. Bull. 73, 707–728.

Dowey, P.J., Hodgson, D.M., Worden, R.H., 2012. Pre-requisites, processes, and prediction of chlorite grain coatings in petroleum reservoirs: A review of subsurface examples. Mar. Pet. Geol. 32, 63–75. doi:10.1016/j.marpetgeo.2011.11.007

Dregne, H.E., 2011. Soils of arid regions. Elsevier.

Du Bernard, X., Carrio-Schaffhauser, E., 2003. Kaolinitic meniscus bridges as an indicator of early diagenesis in Nubian sandstones, Sinai, Egypt. Sedimentology 50, 1221–1229. doi:10.1111/j.1365-3091.2003.00602.x

Eble, C.F., Grady, W.C., 1993. Palynologic and petrographic characteristics of two Middle Pennsylvanian coal beds and a probable modern analogue. Spec. Pap. - Geol. Soc. Am. 286, 119–138.

Edgar, N.T., Cecil, C.B., Mattick, R.E., Chivas, A.R., de Deckker, P., Djajadihardja, Y.S., 2003. A modern analogue for tectonic, eustatic, and climatic processes in cratonic basins; Gulf of Carpentaria, northern Australia. Spec. Publ. - Soc. Sediment. Geol. 77, 193–205.

Eisma, D., 1986. Flocculation and de-flocculation of suspended matter in estuaries. Netherlands J. Sea Res. 20, 183–199.

Fanget, A.-S., Berné, S., Jouet, G., Bassetti, M.-A., Dennielou, B., Maillet, G.M., Tondut, M.,

2014. Impact of relative sea level and rapid climate changes on the architecture and lithofacies of the Holocene Rhone subaqueous delta (Western Mediterranean Sea). Sediment. Geol. 305, 35–53. doi:http://dx.doi.org/10.1016/j.sedgeo.2014.02.004

Fernández-Caliani, J.C., Galán, E., Aparicio, P., Miras, A., Márquez, M.G., 2010. Origin and geochemical evolution of the Nuevo Montecastelo kaolin deposit (Galicia, NW Spain). Appl. Clay Sci. 49, 91–97. doi:10.1016/j.clay.2010.06.006

Folk, R.L., Ward, W.C., 1957. Brazos river bar. A study in the significance of grain size parameters. J. Sediment. Petrol. 27, 3–26.

French, J.R., 1993. Numerical simulation of vertical marsh growth and adjustment to accelerated sea level rise, North Norfolk, UK. Earth Surf. Process. Landforms 18, 63–81. doi:10.1002/esp.3290180105

Geçer Büyükutku, A., Suat Bağcı, A., 2005. Clay controls on reservoir properties in sandstone of Kuzgun formation and its relevance to hydrocarbon exploration, Adana basin, Southern Turkey. J. Pet. Sci. Eng. 47, 123–135. doi:10.1016/j.petrol.2005.03.003

Glennie, K.W., Mudd, G.C., Nagtegaal, P.J.C., 1978. Depositional environment and diagenesis of Permian Rotliegendes sandstones in Leman Bank and Sole Pit areas of the UK southern North Sea. J. Geol. Soc. London 135, 25–34. doi:10.1144/gsjgs.135.1.0025

Harris, P.T., 1988. Large-scale bedforms as indicators of mutually evasive sand transport and the sequential infilling of wide-mouthed estuaries. Sediment. Geol. 57, 273–298. doi:http://dx.doi.org/10.1016/0037-0738(88)90034-6

Hassouta, L., Buatier, M.D., Potdevin, J., Liewig, N., 1999. Clay diagenesis in the sandstone reservoir of the Ellon Field (Alwyn, North Sea. Clays Clay Miner. 47, 269–285.

Henares, S., Caracciolo, L., Cultrone, G., Fernández, J., Viseras, C., 2014. The role of diagenesis and depositional facies on pore system evolution in a Triassic outcrop analogue (SE Spain). Mar. Pet. Geol. 51, 136–151. doi:10.1016/j.marpetgeo.2013.12.004

Horn, D.P., 2006. Measurements and modelling of beach groundwater flow in the swash-zone: a review. Cont. Shelf Res. 26, 622–652. doi:10.1016/j.csr.2006.02.001

Jackson, M.L.R., 1969. Soil Chemical Analysis-Advanced Course. Madison, Wis.

Kantorowicz, J.D., 1990. The influence of variations in illite morphology on the permeability of M. Jurassic Brent Group, Cormorant Field, UK North Sea. Mar. Pet. Geol. 7, 66–74.

Kemp, R.A., Mcdaniel, P.A., Busacca, A.J., 1998. Genesis and relationship of macromorphology and micromorphology to contemporary hydrological conditions of a welded Argixeroll from the Palouse in Idaho. Geoderma 83, 309–329.

Ketzer, J.M., E, R.L.F.D., Dani, N., 2005. Kaolinitic meniscus bridges as an indicator of early diagenesis in Nubian sandstones, Sinai, Egypt – discussion. Sedimentology 52, 213–217. doi:10.1111/j.1365-3091.2004.00685.x

King, G.E., 1992. Formation clays: Are they really a problem in production?, in: Origin, Diagenesis and Petrophysics of Clay Minerals in Sandstones: SEPM Special Publication 47. pp. 265–272.

Kitazawa, T., 2007. Pleistocene macrotidal tide-dominated estuary–delta succession, along the Dong Nai River, southern Vietnam. Sediment. Geol. 194, 115–140.

doi:10.1016/j.sedgeo.2006.05.016

Knaust, D., Bromley, R.G., 2012. Trace Fossils as Indicators of Sedimentary Environments, Developments in Sedimentology. Elsevier Science.

Kranck, K., 1973. Flocculation of suspended sediment in the sea. Nature 246, 348–350.

Kuhn, P., Aguilar, J., Miedema, R., 2010. Textural Pedofeatures and Related Horizons, in: Stoops, G., Marcelino, V., Mees, F. (Eds.), Interpretation of Micromorphological Features of Soils and Regoliths. Elsevier B.V., pp. 217–250. doi:10.1016/B978-0-444-53156-8.00011-8

Le Guern, P., Davaud, E., 2005. Recognition of ancient carbonate wind deposits; lessons from a modern analogue, Chrissi Island, Crete. Sedimentology 52, 915–926. doi:10.1111/j.1365-3091.2005.00700.x

Llana-Fúnez, S., Marcos, A., 2001. The Malpica–Lamego Line: a major crustal-scale shear zone in the Variscan belt of Iberia. J. Struct. Geol. 23, 1015–1030. doi:10.1016/s0191-8141(00)00173-5

McKeague, J.A., Miles, N.M., Peters, T.W., Hoffman, D.W., 1971. A comparison of luvisolic soils from three regions in Canada. Catena 7, 46–69.

Miedema, R., Koulechova, I.., Gerasimova, M.., 1999. Soil formation in Greyzems in Moscow district: micromorphology, chemistry, clay mineralogy and particle size distribution. Catena 34, 315–347. doi:10.1016/S0341-8162(98)00105-2

Moore, D.M., Reynolds, R.C., 1997. X-Ray Diffraction and the Identification and Analysis of Clay Minerals, 2nd ed. ed. Oxford University Press, New York .

Moraes, M.A.S., De Ros, L.F., 1990. Infiltrated clays in fluvial Jurassic sandstones of Recôncavo Basin, northeastern Brazil. J. Sediment. Petrol. 60, 809–819.

Moraes, M.A.S., De Ros, L.F., 1992. Depositional, infiltrated and authigenic clays in fluvial sandstones of the Jurassic Sergi Formation, Reconcavo Basin, northeastern Brazil, in: Origin, Diagenesis and Petrophysics of Clay Minerals in Sandstones: SEPM Special Publication 47. pp. 197–208.

Needham, S.J., Worden, R.H., Cuadros, J., 2006. Sediment ingestion by worms and the production of bio-clays: a study of macrobiologically enhanced weathering and early diagenetic processes. Sedimentology 53, 567–579.

Needham, S.J., Worden, R.H., McIlroy, D., 2005. Experimental production of clay rims by macrobiotic sediment ingestion and excretion processes. J. Sediment. Res. 75, 1028–1037.

Orton, G.J., Reading, H.G., 1993. Variability of deltaic processes in terms of sediment supply, with particular emphasa on grain size. Sedimentology 40, 475–512.

Pérez-Arlucea, M., Álvarez-Iglesias, P., Rubio, B., 2007. Holocene evolution of estuarine and tidal-flat sediments in San Simón Bay, Galicia, NW Spain. J. Coast. Res. 50, 163–167.

Pittman, E.D., Larese, R.E., Heald, M.T., 1992. Clay coats: Occurence and relevance to preservation of porosity in sandstones, in: Houseknecht, D.W., Pittman, E.D. (Eds.), Origin, Diagenesis and Petrophysics of Clay Minerals in Sandstones: SEPM Special Publication 47. SEPM (Society for Petroleum Geology), Tulsa, Oklahoma, pp. 241–255.

Ramm, M., Bjørlykke, K., 1994. Porosity/depth trends in reservoir sandstones: Assessing the quantitative effects of varying pore-pressure, temperature history and mineralogy, Norwegian Shelf data. Clay Miner. 29, 475–490.

Reading, H.G., Collinson, J.D., 1996. Clastic coasts, in: Reading, H.G. (Ed.), Sedimentary Environments: Processes, Facies and Stratigraphy. Blackwell Science, Oxford.

Remy, R.R., 1994. Porosity reduction and major controls on diagenesis of Cretaceous-Paleocene volcaniclastic and arkosic sandstone, Middle Park Basin, Colorado. J. Sediment. Res. A64, 797–806.

Rodrigues Duran, E., di Primio, R., Anka, Z., Stoddart, D., Horsfield, B., 2013. 3D-basin modelling of the Hammerfest Basin (southwestern Barents Sea): A quantitative assessment of petroleum generation, migration and leakage. Mar. Pet. Geol. 45, 281–303. doi:10.1016/j.marpetgeo.2013.04.023

Santos, I.R., Eyre, B.D., Huettel, M., 2012. The driving forces of porewater and groundwater flow in permeable coastal sediments: A review. Estuar. Coast. Shelf Sci. 98, 1–15. doi:10.1016/j.ecss.2011.10.024

Schmid, S., Worden, R.H., Fisher, Q.J., 2004. Diagenesis and reservoir quality of the Sherwood Sandstone (Triassic), Corrib Field, Slyne Basin, west of Ireland. Mar. Pet. Geol. 21, 299–315. doi:10.1016/j.marpetgeo.2003.11.015

Schneider, F., Wolf, S., 2000. Quantitative HC potential evaluation using 3D basin modelling: application to Franklin structure, Central Graben, North Sea, UK. Mar. Pet. Geol. 17, 841–856. doi:10.1016/S0264-8172(99)00060-4

Seemann, U., 1979. Diagenetically formed interstitial clay minerals as a factor in Rotliegend sandstone reservoir quality in the Dutch sector of the North Sea. J. Pet. Geol. 1, 55–62.

Storvoll, V., Bjorlykke, K., Karlsen, D., Saigal, G., 2002. Porosity preservation in reservoir sandstones due to grain-coating illite: a study of the Jurassic Garn Formation from the Kristin and Lavrans fields, offshore Mid-Norway. Mar. Pet. Geol. 19, 767–781.

Tessier, B., Billeaud, I., Sorrel, P., Delsinne, N., Lesueur, P., 2012. Infilling stratigraphy of macrotidal tide-dominated estuaries. Controlling mechanisms: Sea-level fluctuations, bedrock morphology, sediment supply and climate changes (The examples of the Seine estuary and the Mont-Saint-Michel Bay, English Channel, NW Fr. Sediment. Geol. 279, 62–73. doi:http://dx.doi.org/10.1016/j.sedgeo.2011.02.003

Thomson, A., 1979. Preservation of porosity in the deep Woodbine/Tuscaloosa trend, Louisuana. J. Pet. Technol. 34, 396–403.

Umar, M., Friis, H., Khan, A.S., Kassi, A.M., Kasi, A.K., 2011. The effects of diagenesis on the reservoir characters in sandstones of the Late Cretaceous Pab Formation, Kirthar Fold Belt, southern Pakistan. J. Asian Earth Sci. 40, 622–635.

Van Walt Ltd, 2012. Van Walt Window Sampling Factsheet [WWW Document]. URL http://www.vanwalt.com/window-sampling-soil-research.html (accessed 8.31.16).

Varela, M., Prego, R., Pazos, Y., Moroño, Á., 2005. Influence of upwelling and river runoff interaction on phytoplankton assemblages in a Middle Galician Ria and Comparison with northern and southern rias (NW Iberian Peninsula). Estuar. Coast. Shelf Sci. 64, 721–737. doi:10.1016/j.ecss.2005.03.023

Waldmann, S., Gaupp, R., 2016. Grain-rimming kaolinite in Permian Rotliegend reservoir rocks. Sediment. Geol. 335, 17–33. doi:http://dx.doi.org/10.1016/j.sedgeo.2016.01.016

Walker, T.R., Waugh, B., Grone, A.J., 1978. Diagenesis in first-cycle desert alluvium of Cenozoic age, southwestern United States and northwestern Mexico. Geol. Soc. Am. Bull. 89, 19–32.

Walling, D.E., 1999. Linking land use, erosion and sediment yields in river basins. Hydrobiologia 410:, 223–240.

Walling, D.E., 2006. Human impact on land–ocean sediment transfer by the world's rivers. Geomorphology 79, 192–216. doi:10.1016/j.geomorph.2006.06.019

Weibel, R., 1998. Diagenesis in oxidising and locally reducing conditions — an example from the Triassic Skagerrak Formation, Denmark. Sediment. Geol. 121, 259–276. doi:10.1016/S0037-0738(98)00085-2

Weimer, R.J., Howard, J.D., Lindsay, D.R., 1982. Tidal flats and associated tidal channels, in: Scholle, P.A., Spearing, D. (Eds.), Sandstone Depositional Environments. AAPG Memoir, pp. 191–245.

Wilson, I.R., 1998. Kaolin deposits of western Iberia. Geosci. south-west Engl. 9, 214–217.

Wilson, M.D., 1992. Inherited grain-rimming clays in sandstones from eolian and shelf environments: Their origin and control on reservoir properties, in: Origin, Diagenesis and Petrophysics of Clay Minerals in Sandstones: SEPM Special Publication 47. pp. 208–225.

Wilson, M.D., 1994. Non-compositional controls on diagenetic processes, in: Wilson, M.D. (Ed.), Reservoir Quality Assessment and Prediction in Clastic Rocks SEPM Short Course

30. SEPM (Society for Petroleum Geology), pp. 183–208.

Wilson, M.D., Pittman, E.D., 1977. Authigenic clays in sandstones: Recognition and influence on reservoir properties and paleoenvironmental anlysis. J. Sediment. Petrol. 47, 3–31.

Woodroffe, C.D., Mulrennan, M.E., Chappell, J., 1993. Estuarine infill and coastal progradation, southern van diemen gulf, northern Australia. Sediment. Geol. 83, 257–275. doi:http://dx.doi.org/10.1016/0037-0738(93)90016-X

Wooldridge, L.J., Worden, R.H., Griffiths, J., J.E.P., U., n.d. Clay-coated sand grains in petroleum reservoirs: understanding their distribution via a modern analogue. J. Sediment. Res.

Worden, R.H., Needham, S.J., Cuadros, J., 2006. The worm gut; a natural clay mineral factory and a possible cause of diagenetic grain coats in sandstones. J. Geochemical Explor. 89, 428–431.

Figure & table captions

Figure 1. Estuary setting. (A) Country location. (B) Geology of the Anllóns catchment. Estuary geomorphology and core locations and position of correlation transects (Fig. 3).

Figure 2. Photographs of estuary environments. (A) Saltmarsh on the northern side of the estuary dissected by tidal creeks and channels draining on to the intertidal flat. (B) Estuary terrace marking the boundary between saltmarsh and intertidal flat (location marked on Figure 1B. (C) Tidal creeks through partially vegetated muddy intertidal flat (location marked on A). (D) Muddy intertidal flat displaying bioturbation by annelid worms (location marked on A). (E) Partially-vegetated muddy intertidal flat (location marked on A; quadrat is 1 m^2). (F) Sandy intertidal flat displaying bioturbation by annelid worms (location marked on A). (G) Sandy intertidal flat displaying bioturbation and wave ripples (location marked on A; quadrat is 1m^2).

Figure 3. Correlation panels along two estuary transects (locations and orientations marked in Figure 1). The estuary is underlain by sandy intertidal flat (SIF) sediment, in the shallowest part the muddy intertidal flat (MIF) and saltmarsh environments (SS and MS) are present.

Figure 4. Grain coat images of sand grains using binocular microscope. (A) Low resolution images from sample B10 65-70 cm. (B) Low resolution image from B20 0-12 cm. (C) High resolution image from B10 65-70 cm. (D) High resolution image from B20 0-12 cm.

Figure 5. SEM image of stub-mounted, grain-coated sands grains. (A) Low resolution images from sample B10 65-70 cm. (B) High resolution image from B10 65-70 cm. (C) Low resolution image from B20 0-12 cm. (D) High resolution image from B20 0-12 cm. SEM image of thin section, grain-coated sands. (E) Low resolution images from sample B10 65-70 cm. (F) High

resolution image from B10 65-70 cm. (G) Low resolution image from B20 0-12 cm. (H) High resolution image from B20 0-12 cm.

Figure 6. SEM images and energy dispersive X-ray (EDX) spectra (cross marks scan site) of stub-mounted grain coat sand grains from core sample (Qtz: quartz; Ortho: orthoclase). (A, B & C) SEM images of coated sand grain from sample B10 65-70 cm. (D) EDX spectra of coat indicating the presence of kaolinite and pyrite. (E, F & G) SEM images of coated sand grain from sample B20 0-12 cm. (H) EDX spectra of coat indicating the presence of illite, carbonate and pyrite. (I, J & K) SEM images of coated sand grain from sample B20 0-12 cm. (L) EDX spectra of coat indicating the presence of illite, carbonate and trace pyrite.

Figure 7. Thin section SEM images and energy dispersive X-ray (EDX) spectra (cross marks scan site) of grain coats (Qtz: quartz). (A & B) SEM images of coated sand grain from sample B9 75-78 cm. (C) EDX spectra from B9 75-78 cm indicating the presence of chlorite in coat. (D & E) SEM images of coated sand grain from sample B10 65-70 cm. (F) EDX spectra from B10 65-70 cm indicating the presence of illite in coat. (G & H) SEM images of coated sand grain from sample B10 65-70 cm. (I) EDX spectra from B10 65-70 cm indicating the presence of gibbsite in coat. (J & K) SEM images of coated sand grain from sample B13 12.5-22 cm. (L) EDX spectra of B13 12.5-22 cm indicating the presence of kaolinite (and possible trace illite) in the coat and carbonate. (M & N) SEM images of coated sand grain from sample B14 0-14 cm. (O) EDX spectra from B14 0-14 cm indicating the presence of presence of kaolinite in coat.

Figure 8. Weight percentage fine fraction content (red) and mean coat coverage (blue, %) with depth (median sample depth) through each of the twelve cores studied. Cores are ordered in order from most fluvial to most marine from left-to-right and top-to-bottom.

Environment designation (MS, SIF, SS and MIF) refers to the surface environment for that core. Where mean coat coverage values are absent it was not possible to measure coat coverage from the sample. The figure demonstrates that both fine fraction content and mean coat coverage are generally highest in the upper few centimetres of the sediment, with both typically decreasing with increasing depth.

Figure 9. Normalised ternary plots of grain coat XRD mineralogy based on analysis of the fine sediment (< 2 μm fraction; note: this does not represent bulk mineralogy). (A) Plot of total sheet silicates, total framework silicates (feldspar and quartz) and carbonates for the fine fraction (< 2 μm) of the sediment. (B) Plot of individual phyllosilicates: kaolinite, chlorite and illite/muscovite for the fine fraction of the sediment (< 2 μm).

Figure 10. Cross-plot of grain coat versus measured particle size characteristics, depth and fine fraction content. Colours relate to facies designation (Fig. 3). Mean coat coverage (x-axes) are the mean measured coat coverage for each sample. Grain size, skewness and sorting were measured by grain size analysis. Fine fraction content (wt %) was measured by grain size separation techniques.

Figure11. Schematic figure of the likely setting for high initial grain coat coverage (after Dalrymple et al., 1992). Highest initial grain coat coverage is likely to occur in the muddy intertidal flat environment around the margin of the intertidal portion of the estuary where fine-grained sediment is concentrated. Where energies are higher, marine reworking will reduce remove fine-grained sediment from the sandy portions of the intertidal flat. MHT: mean high tide, MLT: mean low tide.

Table 1. Definitions of terms associated with grain coats in clastic sediments

Table 2. Measured grain coat coverage and fine fraction data.

Figure 1
Click here to download high resolution image

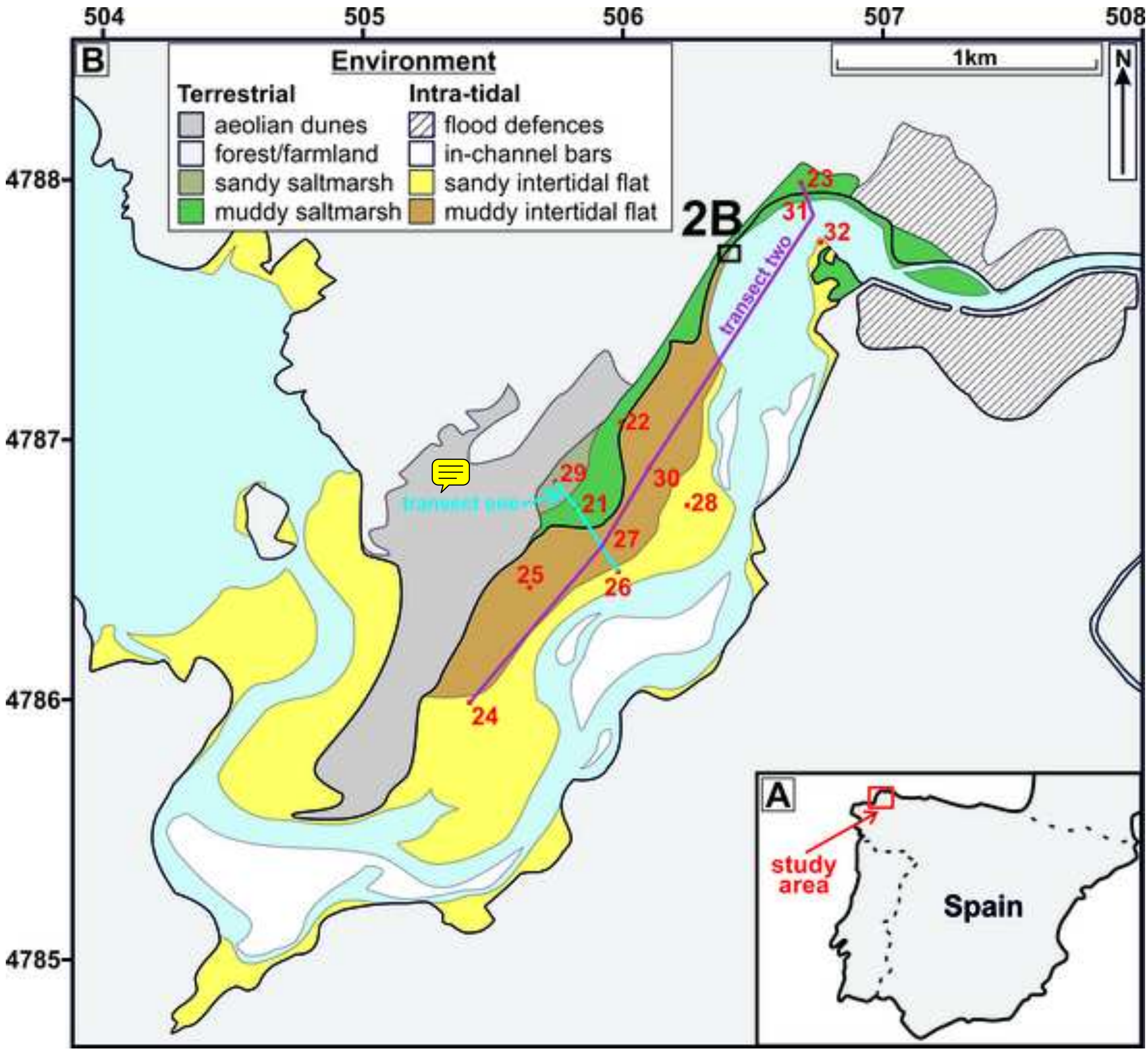

Figure 2
Click here to download high resolution image

Figure 3

Click here to download high resolution image

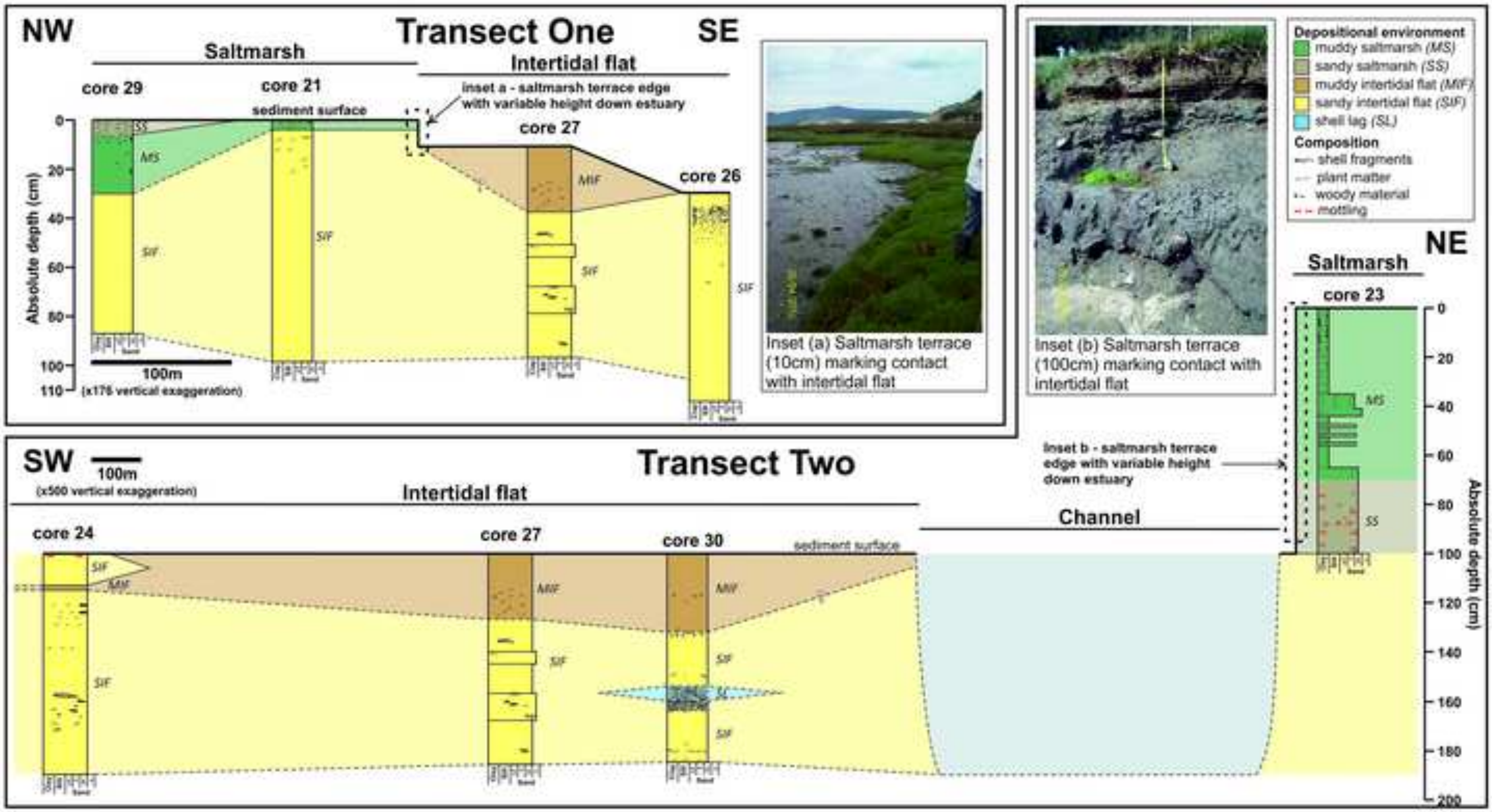

Figure 4
Click here to download high resolution image

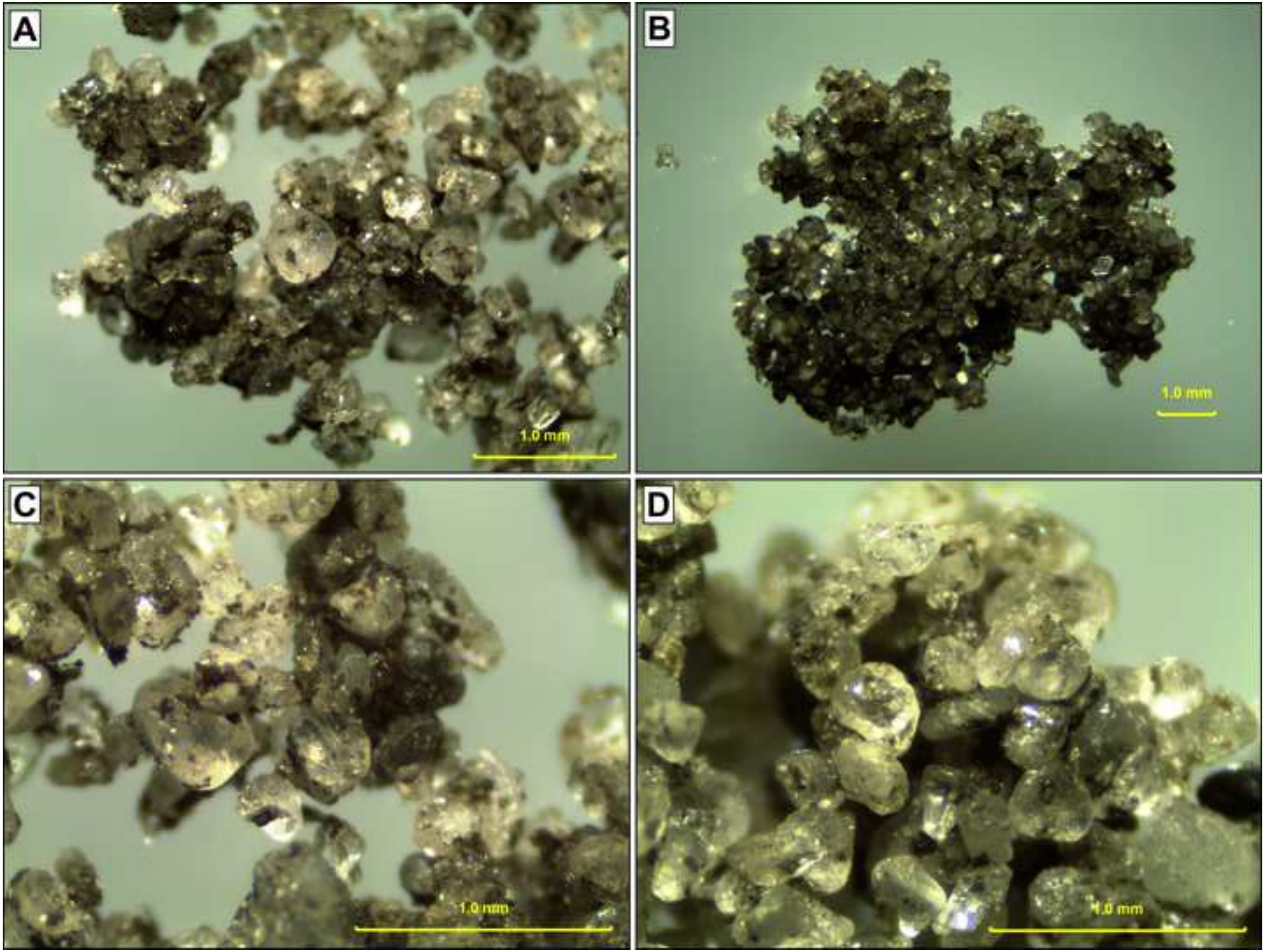

Figure 5
Click here to download high resolution image

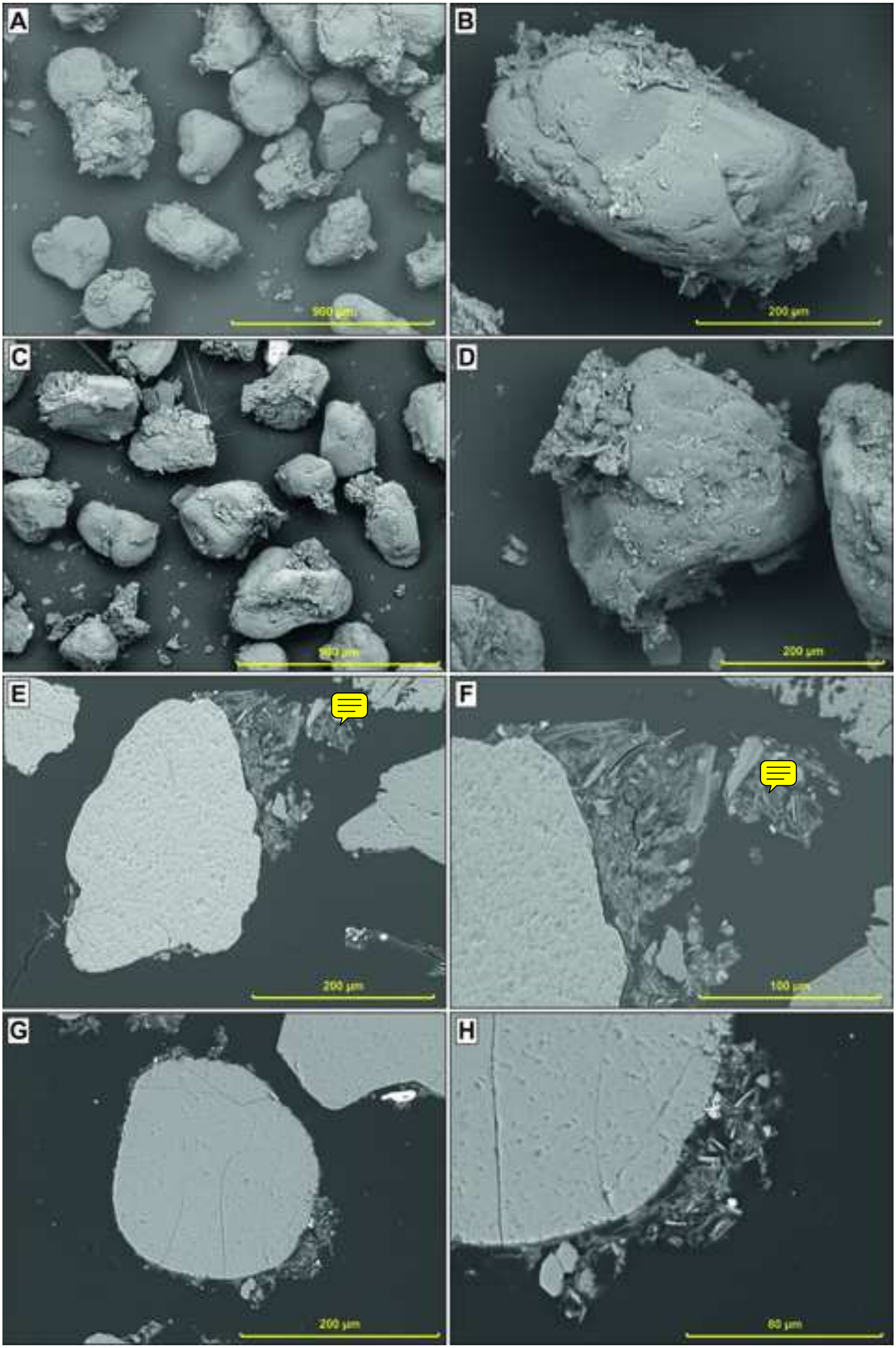

Figure 6
Click here to download high resolution image

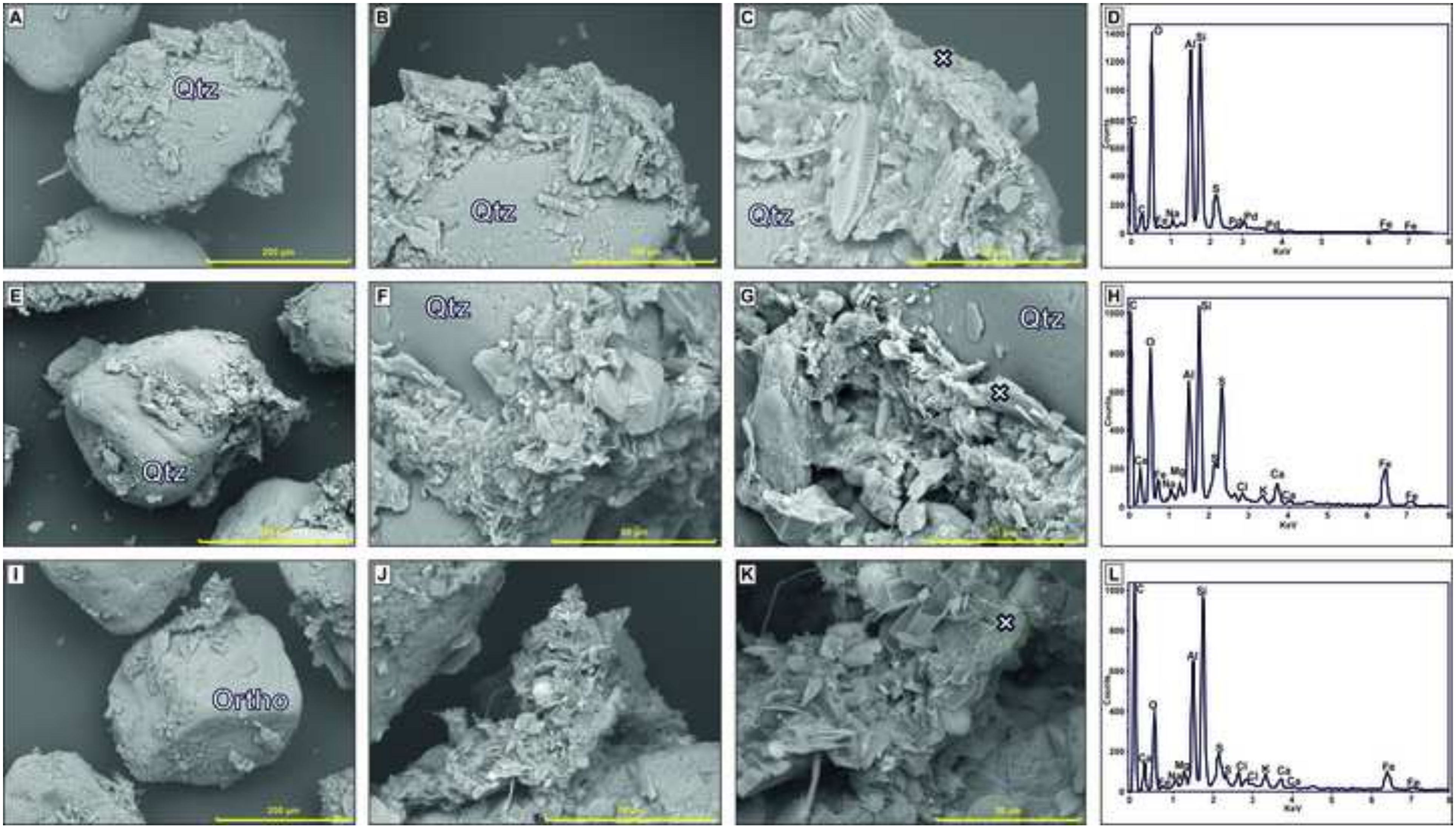

Figure 7
Click here to download high resolution image

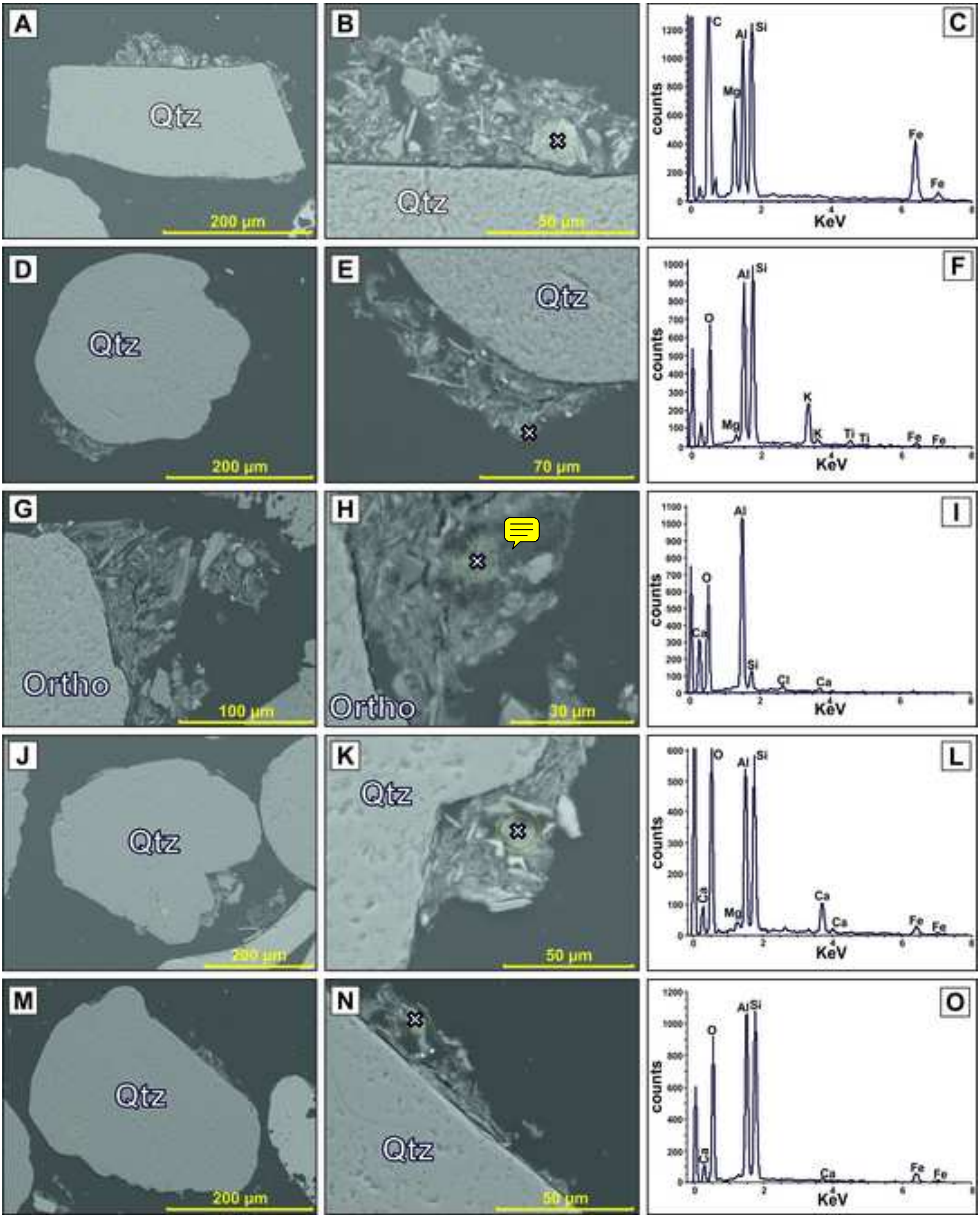

Figure 8
Click here to download high resolution image

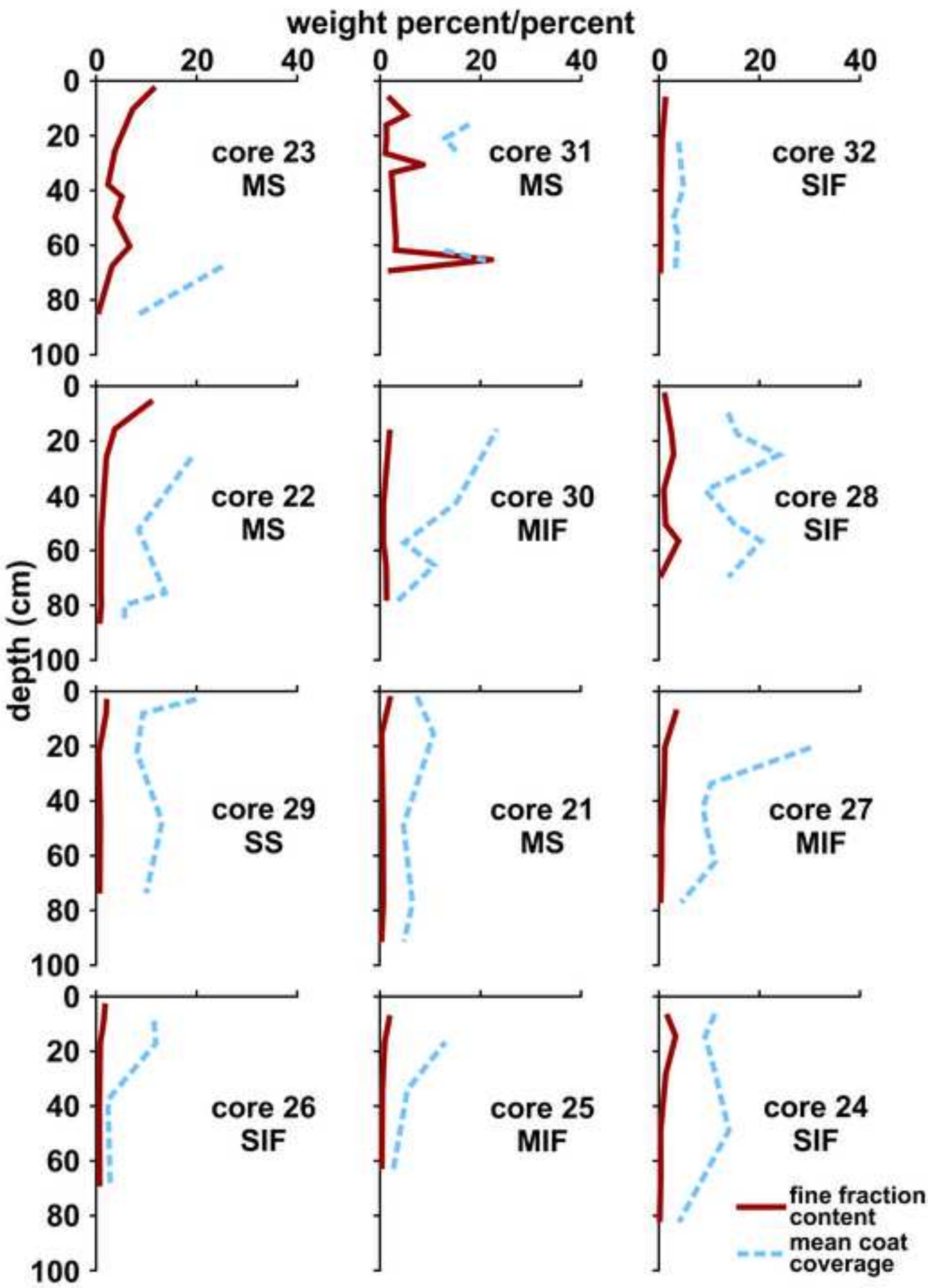

Figure 9
Click here to download high resolution image

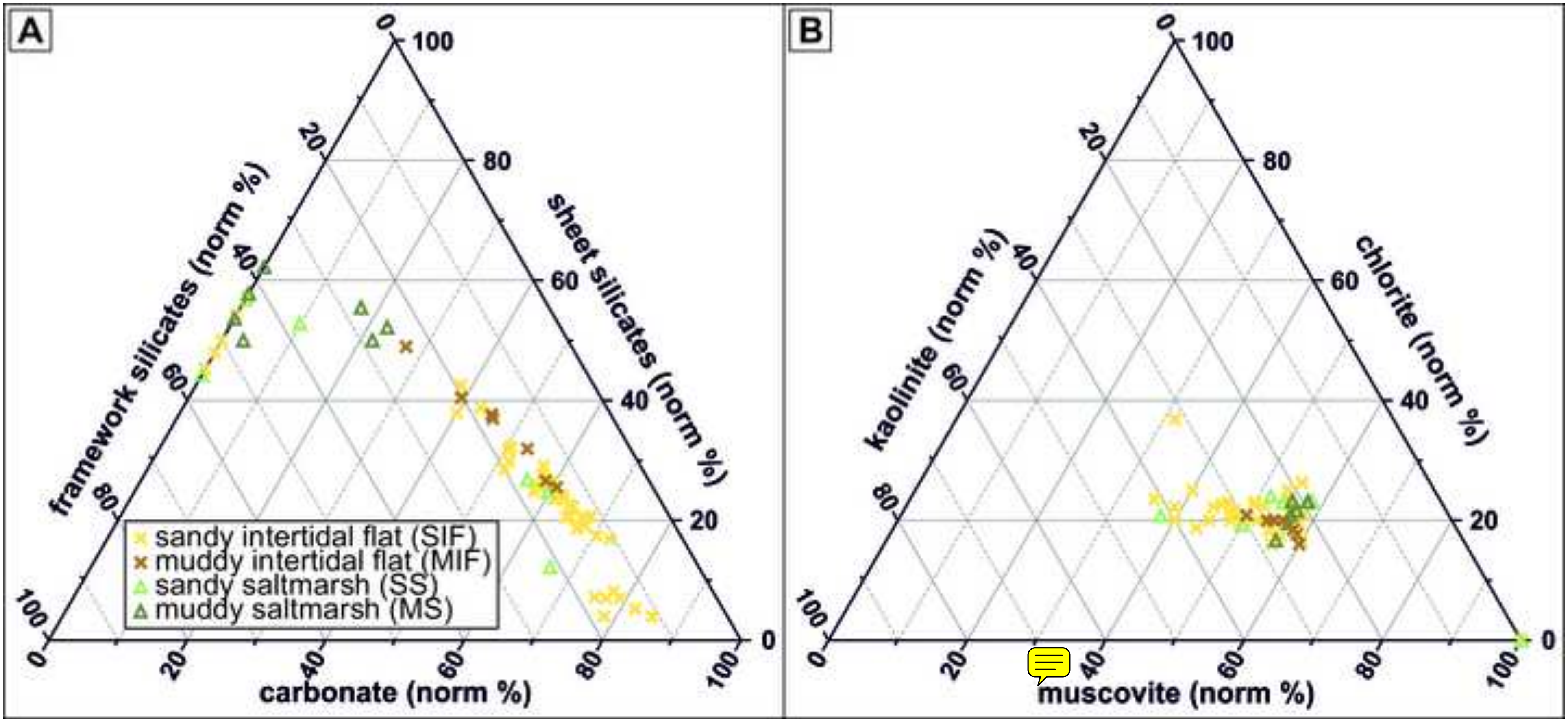

Figure 10

Click here to download high resolution image

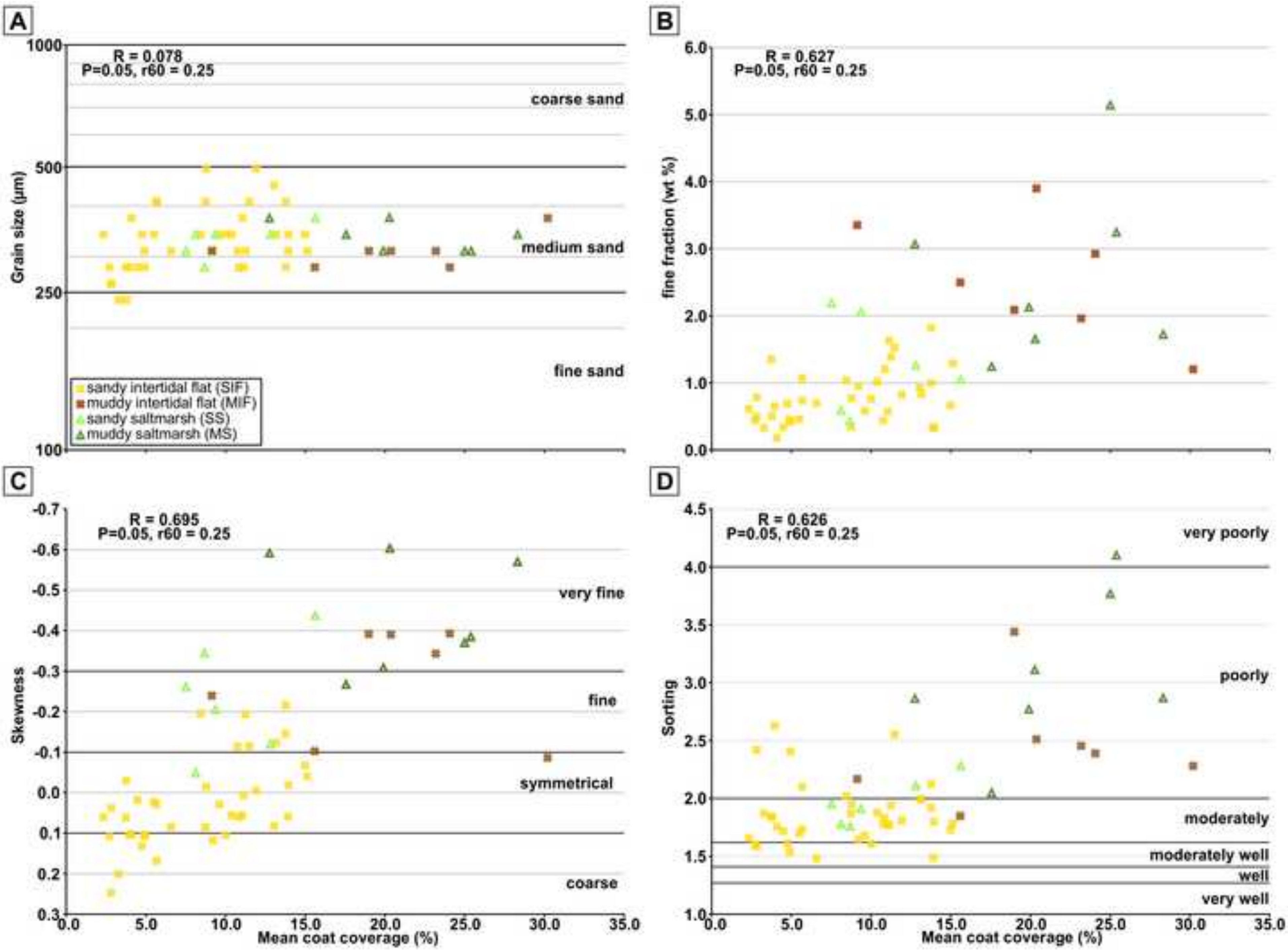

Figure 11
Click here to download high resolution image

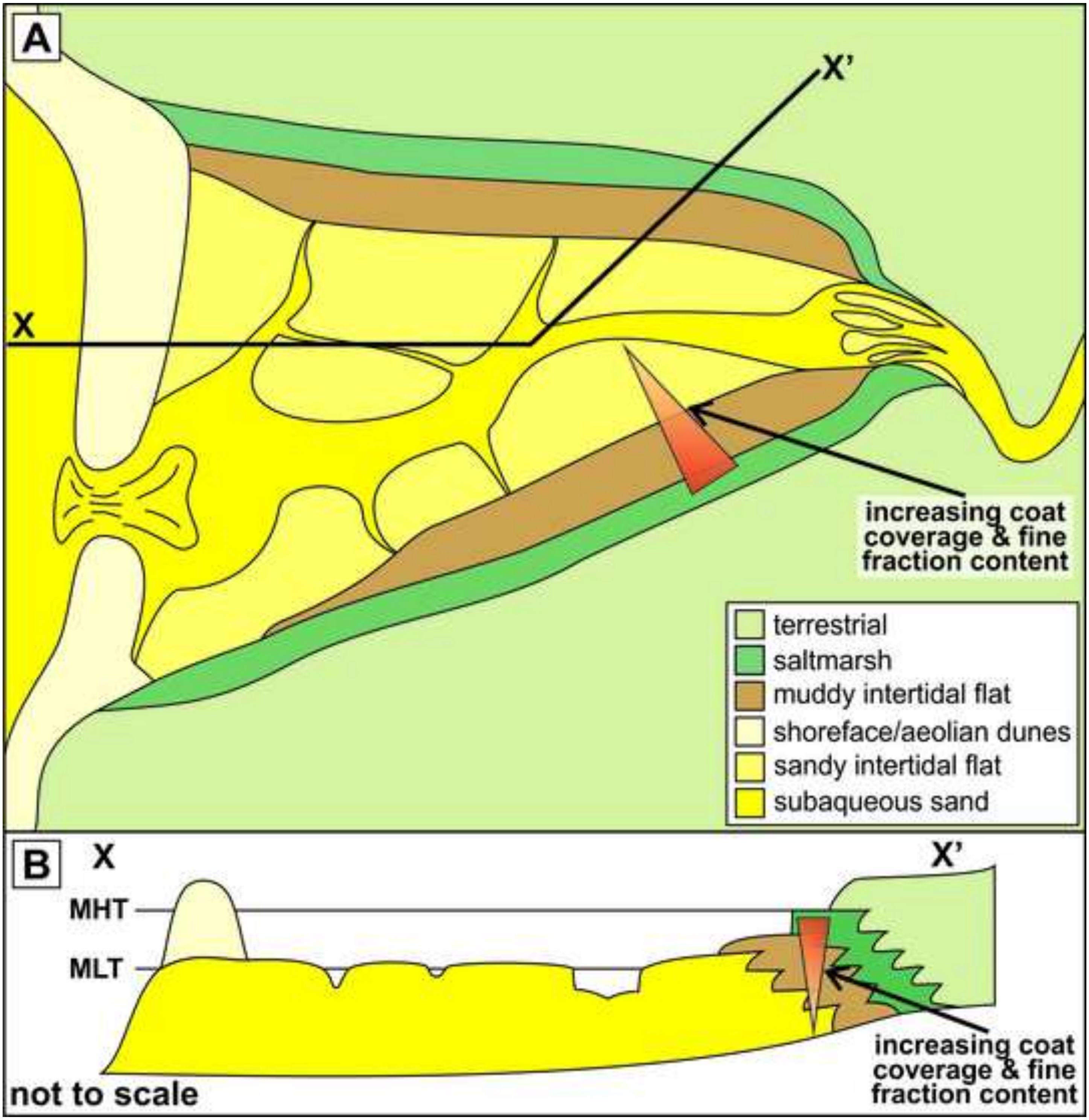

Table 1
Click here to download Table: Table 1.xlsx

Term	**Suggested definition**
Grain coat	Any coat that covers, completely or partially, a sand grain in three dimensions (e.g. like a coat of fur on an animal) found in modern setting or ancient and deeply buried sandstone. A coat has different mineralogy (and/or no crystallographic orientation relationship) to the host grain
Grain rim	A coat on a sand grain observed in *thin section* - giving the appearance of a two dimensional texture (e.g. like the rim of a wheel or the rim of a cup)
Detrital grain coat	A coat on a sand grain (of undefined mineralogy) that formed before, during or immediately after deposition (while still in the depositional environment)
Detrital clay grain coat	A clay mineral-dominated coat on a sand grain that formed before, during or immediately after deposition (i.e. while still in the depositional environment)
Inherited grain coat	A coat on a sand grain (of undefined mineralogy) that formed in a fluvial, or an alluvial, environment prior to deposition and was subsequently transported and deposited in a different sedimentary environment
Inherited clay grain coat	A clay mineral-dominated coat that formed in a fluvial, or an alluvial, environment prior to deposition, and was subsequently transported and deposited in a different sedimentary environment
In-situ grain coat	A coat on a sand grain (of undefined mineralogy) that formed during or immediately after deposition (i.e. while still in the depositional environment)
In-situ clay grain coat	A coat on a sand grain (of undefined mineralogy) that formed during or immediately after deposition (i.e. while still in the depositional environment)
Authigenically-altered detrital grain coat	A coat on a sand grain (of undefined mineralogy) that formed before, during or immediately after deposition, that has been mineralogically modified during shallow burial as the sediment has entered a different geochemical regime (in terms of redox state or water composition)
Authigenically-altered detrital clay grain coat	A clay mineral-dominated coat that formed before, during or immediately after deposition, that has been mineralogically modified during shallow burial as the sediment has entered a different geochemical regime (in terms of redox state or water composition)
Burial diagenetic grain coat	A coat on a sand grain (of undefined mineralogy) that formed during burial and diagenesis (typically > 2,000 m and/or > 70°C)
Burial diagenetic clay grain coat	A clay mineral-dominated coat on a sand grain that formed during burial and diagenesis (typically > 2,000 m and/or > 70°C)
Second-cycle burial diagenetic grain coat	A coat on a sand grain (of undefined mineralogy) that formed during a first cycle of burial and diagenesis in a formation that was then exhumed, eroded, transported and redeposited
Second-cycle burial diagenetic clay grain coat	A clay mineral-dominated coat on a sand grain that formed during a first cycle of burial and diagenesis in a formation that was then exhumed, eroded, transported and redeposited

Table 2
Click here to download Table: Table 2.xlsx

measure	*environment*	*MIF*	*MS*	*SIF*	*SS*
coat coverage (%)	*all samples (100 grains per sample)*				
	n	7	7	39	6
	minimum mean	9.1	12.8	2.3	7.5
	maximum mean	30.2	28.3	15.6	15.6
	mean of means	20.2	21.3	8.4	10.4
	all measured grains				
	n	700	700	3900	600
	minimum	0	0	0	0
	maximum	95	100	80	100
	mean	20.2	21.3	8.4	10.4
	standard deviation	18.0	19.5	10.5	12.5
fine fraction (wt %)	*whole sample*				
	n	7	7	39	6
	minimum	1.2	1.2	0.2	0.4
	maximum	3.9	5.1	1.8	2.2
	mean	2.6	2.6	0.8	1.3
	standard deviation	0.9	1.3	0.4	0.7
modal grainsize (µm)	*whole sample*				
	n	7	7	39	6
	minimum	282.4	310.0	234.3	282.4
	maximum	373.6	373.6	494.2	373.6
	mean	311.2	336.8	334.6	331.1
	standard deviation	30.4	28.5	63.7	31.2
sorting	*whole sample*				
	n	7	7	39	6
	minimum	1.8	2.0	1.5	1.8
	maximum	3.4	4.1	2.6	2.3
	mean	2.4	3.1	1.9	2.0
	standard deviation	0.5	0.7	0.3	0.2
skewness	*whole sample*				
	n	7	7	39	6
	minimum	-0.4	-0.6	-0.2	-0.4
	maximum	-0.1	-0.3	0.2	0.0
	mean	-0.3	-0.4	0.0	-0.2
	standard deviation	0.1	0.1	0.1	0.1

Supplementary material ANOVA

Click here to download Supplementary material for on-line publication only: Supplementary_material_ANOVA.xlsx

Supplementary material Coat XRD
Click here to download Supplementary material for on-line publication only: Supplementary_material_coating_XRD.xlsx